Surface Functionalization of Cotton Fabric with Ag3PO4 via Citric Acid Cross-linking Using An Industrialized Padding Process and Its Self-Cleaning Performance

Yingwen Yan
Tiangong University
Yongchun Dong (teamdong@sina.cn)
Tianjin Polytechnic University
Liran Bian
Tiangong University

Research Article

Keywords: Ag3PO4, Cotton fabric, Industrialized process, Photocatalysis, Self-cleaning

Posted Date: June 7th, 2021

DOI: https://doi.org/10.21203/rs.3.rs-571134/v1

Surface Functionalization of Cotton Fabric with Ag_3PO_4 via Citric Acid Cross-linking Using An Industrialized Padding Process and Its Self-cleaning Performance

Yingwen Yan[a], Yongchun Dong[a,b*], Liran Bian[a]

[a] Division of Textile Chemistry & Environmental Care, School of Textile Science & Engineering, Tiangong University, Tianjin 300387, China

[b] Key Laboratory of Advanced Textile Composite of Ministry of Education, Tiangong University, Tianjin 300387, China

***Corresponding author:**

Prof. Yongchun Dong

Division of Textile Chemistry & Environmental Care

School of Textile Science & Engineering, Tiangong University

399 Binshui West Road, Xiqing District, Tianjin 300387, P. R. China

Post code: 300387

Tel/Fax: 86-22-83955359

E-mail: teamdong@sina.cn or dye@tiangong.edu.cn

Abstract

Cotton fabric was first modified with citric acid to introduce surface carboxyl groups, which then coordinated with Ag^+ ions to prepare the Ag_3PO_4 finished cotton fabric through further reacting with PO_4^{3-} ions using an industrialized pad-dry-cure process. Increasing surface carboxyl groups could significantly enhanced the loaded content of Ag_3PO_4. The padding process could more strongly fix Ag_3PO_4 on fabric than the conventional dipping method. The Ag_3PO_4 finished cotton fabric showed higher photocatalytic capacity than pure Ag_3PO_4 particles owing to the synergetic effect of the Ag complex with the carboxyl groups on the fabric. Moreover, the treatment of KBr and fixing agent further improved the the stability and anti-photocorrosion performance of the samples. Importantly, the finished fabric also exhibited better self-cleaning performance for Reactive Red 195 as a model stain under varied irradiation. The dye was found to be decomposed and mineralized on the finished fabric under artificial or solar irradiation.

Keywords: Ag_3PO_4; Cotton fabric; Industrialized process; Photocatalysis; Self-cleaning

1 Introduction

Semiconductor photocatalysts have drawn great attention for the last 30 years because of their typical structures, excellent characteristic properties and potential applicability in environmental pollutants degradation and solar energy harvesting. Among various oxide-based semiconductor photocatalysts, TiO_2 nanoparticles have been provided to be one of the best photocatalysts in a lot application sectors, including environmental care, self-cleaning and antibacterial because of their high oxidation capacity, better chemical stability, low toxicity and cost-effectiveness (Burunkaya et al. 2013; Ji et al. 2010; Kamegawa et al. 2011; Lucas et al. 2013). However, the major disadvantages of many semiconductor photocatalysts are that their photocatalytic activity greatly limited owing to the fast recombination of photoexcited carriers and the low efficiency in solar energy utilization. Especially, TiO_2 nano particles show poor performance in utilizing visible light as irradiation source for photocatalysis because they possess wide band gap energy (3.2 eV) and only be excited by ultravioletlight (wavelength < 388 nm), which accounts for about 4% of solar irradiation (Cai et al. 2014; Wang et al. 2013). In recent ten years, silver phosphate (Ag_3PO_4) has been studied as an important visible light-driven photocatalyst due to its relatively narrow band gap energy (about 2.43 eV), thus absorbing ultraviolet light and visible light with a wavelength shorter than 530 nm (Bi et al. 2011; Guo et al. 2017; Yi et al. 2011). In addition, the valence band of Ag_3PO_4 is approximately +2.9 V vs. NHE, suggesting that it shows high photocatalytic capacity to decompose organic compounds in aqueous system under visible light irradiation (Yu et al. 2017). Unfortunately, several weaknesses have been found in the Ag_3PO_4 photocatalytic system (Chen et al. 2016; Li et al. 2015; Song et al. 2018): (1) there is the uncontrollable photocorrosion under light irradiation during its reaction process, especially without electron acceptors, thus leading to a reduced stability and activity of

Ag_3PO_4 in water. (2) small size of Ag_3PO_4 nanoparticles usually show high photocatalytic activity, which may result in a difficult separation of the nanoparticles from water, thus causing secondary pollution. (3) relatively high cost of $AgNO_3$ as the starting material may limits the large-scale preparation and application of Ag_3PO_4 photocatalyst in the future. To address these issues, It has been reported that loading and dispersing of Ag_3PO_4 particles on some semiconductor materials (Lin et al. 2012; Yao et al. 2012; Yang et al. 2013) or suitable organic support materials, especially different fibers (Cai et al. 2014; Panthi et al. 2017; Wang et al. 2014; Xiong et al. 2018; Yu et al. 2013) to build unique composite structures or heterojunction systems is an optional way to enhance its photocatalytic performance and stability. However, the information about impact of organic polymers on photocatalytic activity of Ag_3PO_4 has been very limited. Furthermore, it is a serious challenge to incorporate Ag_3PO_4 photocatalyst onto organic polymers using industrialized processes for developing its practical application. Recent literature (Panthi et al. 2017; Wang et al. 2014; Xiong et al. 2018; Yu et al. 2013) revealed that although the loading of Ag_3PO_4 particles on fibrous materials for photocatalysis has been reported, the loading methods used were usually hand operation or crude processes, especially dipping and electrospinning without modern industrialized equipment, which may result in an undesired formation of Ag_3PO_4 particles on the fibrous materials, thus blocking their future commercial application. Thus, it is expected that production of large-scale fiber based Ag_3PO_4 photocatalyst can be developed through industrialized methods for enhancing its applied possibility. In our present study, cotton fabric was modified with citric acid to introduce surface carboxylic groups, which were then used to fix the formed Ag_3PO_4 particles through the coordination of carboxylic groups and Ag^+ ions via a regular industrialized pad-dry-cure finishing process since cotton fiber show a hierarchical network structure with hydrophilic groups and high

porosity (Li et al. 2015; Pasta et al. 2010; Shen et al. 2016), which may favor the adsorption of the formed Ag_3PO_4 particles on its surface. Besides, it is well known that pad-dry-cure process is the most important continuous large-scale production method for contemporary textile dyeing and finishing. This process not only accomplished the surface carboxyliztion of cotton fiber with citric acid, but also enhanced the even and tight loading of the formed Ag_3PO_4 particles on its surface by high-powered padding and low temperature dry steps in this work. Several main factors effecting Ag_3PO_4 loading process, such as surface carboxylic group content of the modified fabric, $AgNO_3$ and Na_2HPO_4 concentration and pad-dry-cure process conditions were also investigated. And then the Ag_3PO_4 finished cotton fabric was tested for photocatalytic activity. The enhanced effect of the formed Ag complex on the photocatalytic activity and stability of the Ag_3PO_4 finished cotton fabric was discussed. A commonly used azo dye, Reactive Red 195 was used as a model stain to evaluate and compare the self-cleaning performance of the Ag_3PO_4 finished cotton fabric under different irradiation. A detail degradation route of the dye stain on the sample was also investigated and proposed during the self-cleaning process.

2 Experimental section

2.1 Materials and agents

A commercial cotton woven fabric (208.4 gm^{-2}) was used in this investigation. Citric acid, $AgNO_3$, Na_2HPO_4, NaH_2PO_4, KBr and N,N-dimethylformamide were analytical grade and employed without any treatment. A typical commercial azo dye, Reactive Red 195 (RR 195, CAS: 93050-79-4) was used, and its molecular structure was displayed in Scheme 1. Distilled water was obtained by a quartz sub-boil high purity water distiller and used throughout the work.

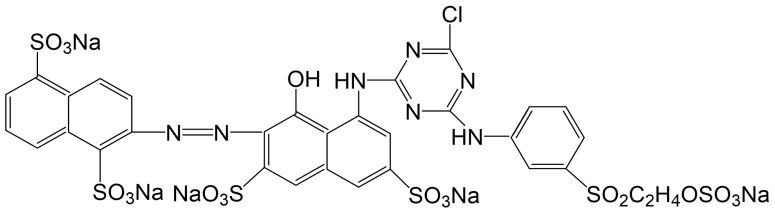

Scheme 1 Molecular structure of RR 195

2.2 Finishing of cotton fabric with Ag_3PO_4 particles

2.2.1 Surface carboxylation of cotton fabric with citric acid

Cotton fabric was modified with citric acid (CA) to introduce carboxyl groups on its surface via an regular pad-dry-cure process reported in our previous study (Li et al. 2015). In a typical procedure, cotton fabric was padded twice with an aqueous solution containing different concentration of CA and NaH_2PO_4 as a catalyst at air temperature on a two-roll laboratory mangle to give a wet pick-up of 70-75% based on the weight of fabric. And then the padded fabric was dried at 85℃ for 4.5 min and cured at 180℃ for 1.5 min to achieve a carboxylated cotton fabric (denoted as CA-Cotton). After being rinsed with deionized water thoroughly and dried under vacuum, the obtained CA-Cotton was tested for surface carboxyl group content (Q_{COOH}, $mmolg^{-1}$) by an acid-base titration method (Li et al. 2015). The reaction of cotton fiber with CA at cure stage was expressed though Scheme 2.

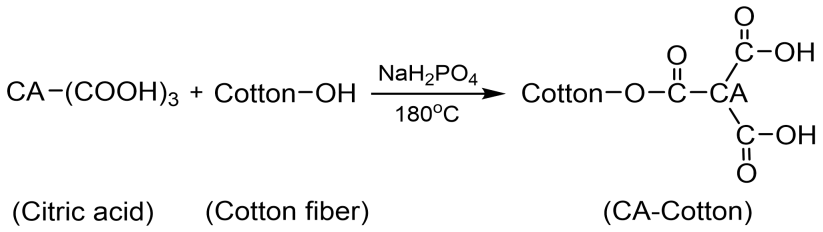

Scheme 2 Esterification of cotton fiber with CA during pad-dry-cure process

2.2.2 Immobilization of Ag_3PO_4 on cotton fabric

CA-Cotton sample was padded twice (pick-up: 70-75%) with the known concentration of $AgNO_3$ aqueous solution on the laboratory mangle used above, and then dried at 80℃ for 5 min. Afterward,

the resulting sample was treated with different concentration of Na_2HPO_4 aqueous solution through the same pad-dry process. Finally, the treated sample was cured at 120℃ for 2 min, then thoroughly rinsed with deionized water and dried to get the finished Ag_3PO_4 cotton fabric (named as Ag_3PO_4@CA-Cotton). To measure Ag_3PO_4 content loaded on cotton fabric, Ag_3PO_4@CA-Cotton was completely dissolved in concentrated HNO_3, and then the concentration of Ag^+ ions in the resulting solution was determined using a Varian Vista-MPX inductively-coupled plasma optical emission spectroscopy (ICP-OES). Ag_3PO_4 content (Q_{SP}, $mmolg^{-1}$) loaded on cotton fabric could be calculated through Equation (1), since the amount of Ag^+ ions reacted with CA-Cotton was so small that it was neglected. Additionally, the loading strength (L_{SP}) of Ag_3PO_4 particles on cotton fabric was also evaluated through a regular washing test according to Textiles Test Specification for Color Fastness (GB/T3921-2008, ISO105-C10: 2006). In a washing test process, 2.0 g of dried sample was immersed into a 100 mL of 5.0 gL^{-1} soap aqueous solution and then agitated (1000 $rmin^{-1}$) for 40 min at 50℃. All the samples were washed three times. At the end of the third wash cycle, the samples were rinsed thoroughly with deionized water and dried. L_{SP}% value of the sample was expressed by Equation (2).

$$Q_{SP} = \frac{C_{Ag} V}{M_{Ag} \times 3 \times W} \times 100\% \qquad (1)$$

where C_{Ag} was the concentration of Ag^+ ions in HNO_3 solution (mgL^{-1}), V was the HNO_3 solution volume (L), M_{Ag} was molecular weight of silver (107.9), and W was the weight of Ag_3PO_4@CA-Cotton (g).

$$L_{SP} = \frac{W_A}{W_B} \times 100\% \qquad (2)$$

where W_B and W_A were the weight of Ag_3PO_4@CA-Cotton before and after washing test (g),

respectively.

2.3 Characterization of Ag_3PO_4@CA-Cotton

S-4800 Field-emission scanning electron microscopy (Hitachi High-Tech Co., Japan) was adopted by operating at 15 kV to investigate the surface morphology of Ag_3PO_4@CA-Cotton. The crystal structure of the Ag_3PO_4 finished cotton fabric was analyzed through a D8 Advance Bruker diffractometer using Cu Kα irradiation source at 40 kV and scan range 5-80^o with a scan speed of 2^o/min. The surface molecular composition of Ag_3PO_4@CA-Cotton was analyzed using a VERTEX 70 FTIR spectrometer ranging from 450 to 3800 cm^{-1}.The core level spectra of several elements of the samples were carried out on a PHI 5600 X-ray photoelectron spectrometer (Pekin-Elmer Inc., USA), and the binding energy of C1s was shifted to 284.8 eV as the reference. The light adsorption properties of the samples were also evaluated by measuring their diffuse reflectance UV-vis spectra (DRS), which were recorded on a Varian Cary 500 UV-vis-NIR spectrometer (Varian Inc., USA) in the 200-800 nm wavelength range with $BaSO_4$ as the reflectance standard.

The electrochemical analysis of Ag_3PO_4@CA-Cotton was conducted by a CHI660D electrochemical work station (Shanghai Chenhua Instruments Co., China) in a standard three electrode system. For photocurrent measurements, Pt plate and Ag/AgCl electrode were used as the counter electrode and reference electrode, respectively. To prepare working electrode, Ag_3PO_4 particles were removed from Ag_3PO_4@CA-Cotton surface, and then dispersed in DMF solution to produce a colloidal solution (1.0 $mgmL^{-1}$) and treated by ultrasonication for the desired time. Subsequently, 0.10 mL of the obtained solution was dropped on the pretreated FTO glass, and then which was dried under vacuum conditions. Moreover, a Na_2SO_4 aqueous solution (0.20 M) was used as the electrolyte. The white light-emitting LED lamp was adopted as visible light source. For

Mott-Schottky measurement, an impedance-potential model was used for investigating the band positions of the samples.

2.4 Photocatalytic activity test

Photocatalytic activity of Ag_3PO_4@CA-Cotton was evaluated through measuring the degradation rate of RR 195 in water with Ag_3PO_4@CA-Cotton as the photocatalyst under LED visible irradiation. The whole degradation experiments were performed in a self-made photoreaction system reported in our earlier work (Dong et al. 2010). It was mainly made up of chamber, water bath, relay and electromagnetic valve. 100ml open Pyrex vessels were used as reaction receivers in water bath. The irradiation intensity over the vessels was tested from LED visible light source inside of the system. 30 mL of test solution containing 0.025 $mmolL^{-1}$ RR 195 and 1.0 g of Ag_3PO_4@CA-Cotton sample pieces were added into the vessels, and then uninterruptedly agitated at pH 3 and 25℃ under irradiation for dye degradation. During the reaction, RR 195 concentration was determined by sampling at the different times and then analyzed using a UV-2401 Shimadzu spectrophotometer at 522 nm (maximum absorption wavelength of RR 195 in water according to a calibration curve prepared earlier. The decoloration percentage (D%) of RR 195 at a given time was calculated by Equation 3.

$$D\% = \frac{C_{d,0} - C_d}{C_{d,0}} \times 100\% \qquad (3)$$

where $C_{d,0}$ and C_d are the initial and residual concentration of RR 195 ($mmolL^{-1}$), respectively. The high D% value indicated the strong photocatalytic activity of Ag_3PO_4@CA-Cotton.

2.5 Self-cleaning study

Self-cleaning capacity of Ag_3PO_4@CA-Cotton was examined through assessing the decoloration efficiency of Ag_3PO_4@CA-Cotton dyed with RR 195 as model color stain when being exposured to

artificial light or solar irradiation. The dye stained fabric was prepared by immersing 1.5 g of Ag_3PO_4@CA-Cotton sample in 100 mL of RR 195 aqueous solution (0.50 gL^{-1}) for 24 h at ambient temperature. Afterward, the resulting fabric was removed from the solution and was dried in a vacuum at 60℃ for 5 h. When Fluorescent/UV Instrument (UV Test®, USA) being used as artificial light source, dye stained fabric was exposed vertically to UV radiation with 0.70 Wcm^{-2} at 340 nm at air temperature. Solar light experiment was performed at 20-30℃ using the glass plate held in a rack at a 30° angle from the horizontal on the top of lab building at the campus of Tiangong University located at Xiqing District in Tianjin city. During the test procedure, the solar light intensity was continually recorded using FZ-A radiometer and UV-A radiometer. To increase self-cleaning test efficiency, a specially designed photocatalytic self-cleaning test system was used to shorten the time limit for the test. This system consisted mainly of a 141 L organic glass lined with aluminum foil chamber, 250 W high voltage halogen lamp as a light source, circulation air fan, temperature controller and vertical lifting sample stage. Its schematic picture was described in Fig. 1.

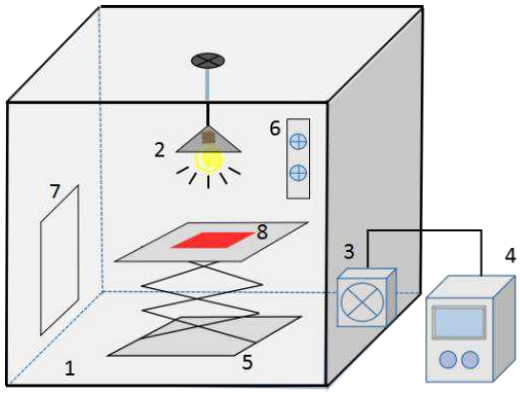

Fig. 1 Diagrammatic sketch of photocatalytic self-cleaning test system: (1) test chamber, (2) high voltage halogen lamp, (3) circulation air fan, (4) temperature controller, (5) vertical lifting sample stage, (6) temperature and humidity indicator, (7) sampling gate, (8) test sample

During the self-cleaning test, the dye stained fabric was got out of the system after irradiated for

different periods, and then extracted repeatedly with deionized water under constant agitating at 60℃ for 20 min to remove all the dye and its degradation products from the stained fabric to water bath. Subsequently, the resulting extract liquids were collected and filtered for the UV-visible spectrometric analysis and TOC (Total organic content) measurement. The decomposition percentage (D_E%) and TOC removal percentage (TOC_R%) of RR 195 were calculated to assess the self-cleaning performance of the samples. Generally, the greater the D_E% and TOC_R% values, the better the self-cleaning performance of the samples. Both values were expressed through Equations 4 and 5. To investigate the photocatalytic degradation route of RR 195 on Ag_3PO_4@CA-Cotton sample during the the self-cleaning test, the extract liquid was also analyzed by GC-MS with an Agilent HP 6890 N chromatograph equipped with a DB-5 capillary column combined with an Agilent 5973 N mass spectroscopy to detect the main degradation intermediates generated from the dye decomposotion during the test.

$$D_E\% = \frac{C_{e,0} - C_e}{C_{e,0}} \times 100\% \qquad (4)$$

where $C_{e,0}$ and C_e are the concentration of RR 195 ($mmolL^{-1}$) in the extract liquid before and after irradiation for a certain time, respectively.

$$TOC_R\% = \frac{TOC_0 - TOC}{TOC_0} \times 100\% \qquad (5)$$

where TOC_0 and TOC are the TOC values of the extract liquid before and after irradiation for a certain time, respectively.

3 Results and discussion

3.1 Generation and loading of Ag_3PO_4 particles on cotton fabric

CA-Cotton samples with different Q_{COOH} values were treated with $AgNO_3$ and Na_2HPO_4 aqueous

solutions alternately through pad-dry-cure process to prepare a series of Ag_3PO_4@CA-Cotton. Q_{SP} and L_{SP}% values of the resulting samples were then measured and presented in Fig. 2.

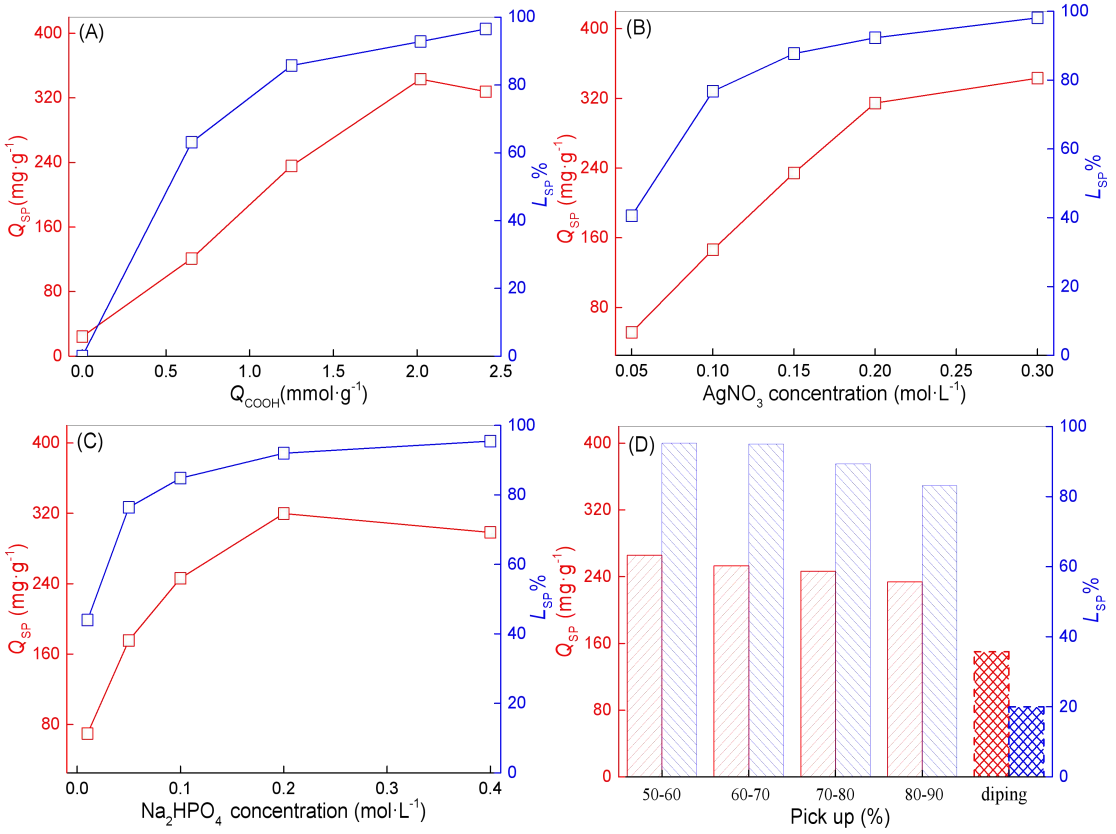

Fig. 2 Effect of finishing process on Q_{SP} and L_{SP}% values of Ag_3PO_4@CA-Cotton

It was shown in Fig. 2(A) that high Q_{COOH} level significantly increased Q_{SP} and L_{SP}% values, indicating that increasing the content of surface carboxyl groups on cotton fabric favored the reaction of Ag^+ between PO_4^{3-} ions and the immobilization of the resulting Ag_3PO_4 particles on its surface. This was mainly because that Ag^+ ions could not only react with PO_4^{3-} ions to generate Ag_3PO_4 (Jiao et al. 2012; Li et al. 2019), but also coordinate with carboxyl groups in the structure of many compounds (Curran and Sc 2009; Whitcomb and Rajeswaran 2006). It is known that carboxylate is one of the most important O-donor ligands for complexation with silver(I) since the carboxyl group has four lone pairs of electrons on the two oxygen atoms, which are available for metal binding (Curran and Sc 2009). On the other hand, silver show four oxidation states, with Ag(I) being the

most common. The spherically symmetric configuration of the Ag(I) ion allows the coordination number to vary from 2-6. Argentophilicity is the tendency of Ag(I) ions to aggregate at distances below the van der Waals diameter of 3.44 Å. The Ag(I)···Ag(I) interactions can be responsible for the structural arrangement of crystals (Whitcomb and Rajeswaran 2006; Young and Hanton 2008). Moreover, some coordination polymers have be found to contain Ag-Ag bonds with mono and bidentate chelation of the carboxyl groups (Zhu et al. 2003). Importantly, it was confirmed that citrate ions could form a silver complex with silver ions as [Ag_2--citrate] or $[Ag_3(C_6H_5O_7)_{n-1}]^{3n-}$ in the aqueous solution (Jiang et al. 2010). Accordingly, it is believed that Ag^+ ions may simultaneously combine with PO_4^{3-} ions and carboxyl groups on cotton fiber, thus leading to the better attachment of the formed Ag_3PO_4 particles to the fabric in this work (Scheme 3). Moreover, increasing Q_{COOH} value offered much more carboxyl groups on the fiber, which reacted with Ag^+ ions easily through intermolecular or intramolecular coordination to immobilize more Ag_3PO_4 particles on the fiber.

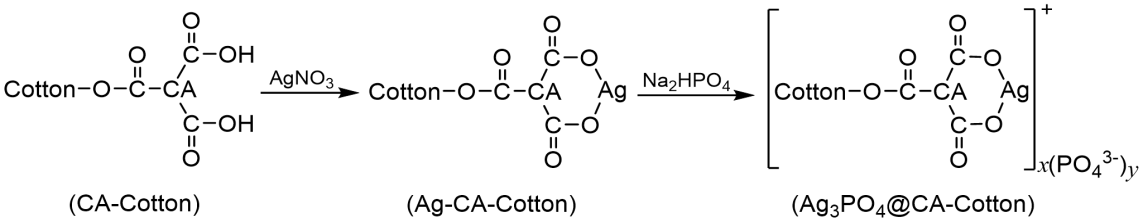

Scheme 3 A possible reaction mode of Ag^+ ions with PO_4^{3-} ions and surface carboxyl groups of CA-Cotton

Fig. 2(B) and (C) showed the enhanced effect of $AgNO_3$ and Na_2HPO_4 concentration on Q_{SP} and L_{SP}% values. A main reason was that increasing concentrations of $AgNO_3$ and Na_2HPO_4 in the solution promoted the contact between Ag^+ and PO_4^{3-} ions, thus enhancing the formation of Ag_3PO_4 particles on cotton fabric. Besides, high concentration of Ag^+ ions may improve the deposition strength of the formed Ag_3PO_4 particles on cotton fabric through increasing the coordination of Ag^+

ions with carboxyl groups. As shown in Fig. 2(D), comparing with regular dipping method, industrialized padding process was adopted to obtain higher Q_{SP} and L_{SP}% values. Moreover, increasing mangle roller pressure (decreasing take up%) caused a gradual increment in Q_{SP} and L_{SP}% values. These demonstrated that padding process could obviously improve the formation and deposition of Ag_3PO_4 particles on cotton fabric. This may be attributed to the fact that padding roller pressure could enhance the penetration of $AgNO_3$ and Na_2HPO_4 solution into cotton fabric when padding process being used, which would be in favor of the reaction of Ag^+ ions with PO_4^{3-} ions and carboxyl groups inside cotton fibers, thus further accelerating the adsorption of the generated Ag_3PO_4 particles onto the fabric. These finds provided a new strategy to develop and apply Ag_3PO_4-based photocatalysts on a massive scale in the day to come. In order to further improve the fixation of Ag_3PO_4 particles onto the fabric, Ag_3PO_4@CA-Cotton was treated with KBr and pseudocationic active fixing agent aqueous solutions using the pad-dry process in succession before washing test, and then Q_{SP} and L_{SP}% values of the obtained samples after washing test were showed and compared in Fig. 3.

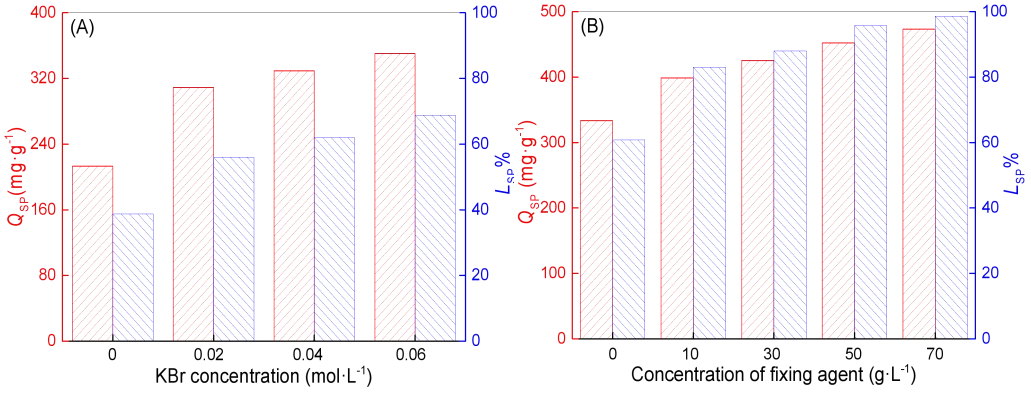

Fig. 3 Enhanced effect of KBr (A) and fixing agent (B) on loading of Ag_3PO_4 on cotton fabric

When Ag_3PO_4@CA-Cotton was treated with only KBr solution, increasing KBr concentration was accompanied with an increment in Q_{SP} and L_{SP}% values (Fig. 3A). This was mainly due to much

lower solubility of AgBr than Ag_3PO_4, which were in intimate contact with the outer surface of Ag_3PO_4 crystals, preventing their dissolution in aqueous solution (Bi et al. 2011). In case of treating with both KBr (0.06 $molL^{-1}$) and fixing agent, Q_{SP} and L_{SP}% values rose with increasing concentration of fixation agent, and they were closed to 500 mgg^{-1} and 100%, respectively at the concentration of 70 gL^{-1}. This was because fixing agent was prepared through the amidation of the condensate resin of polyethylene-polyamine with dicyandiamide to introduce the hydroxymethyl groups, which could react with the hydroxyl groups of cotton fiber to form stable ether bondings (Wang et al. 2018), thus limiting Ag_3PO_4 particles from moving out of the fiber. Besides, fixing agent could produce a polymer layer near the fiber surface to encapsulate Ag_3PO_4 particles for reducing their ability to diffuse out of the fiber during water washing.

3.2 Characterization of Ag_3PO_4@CA-Cotton

3.2.1 SEM observation

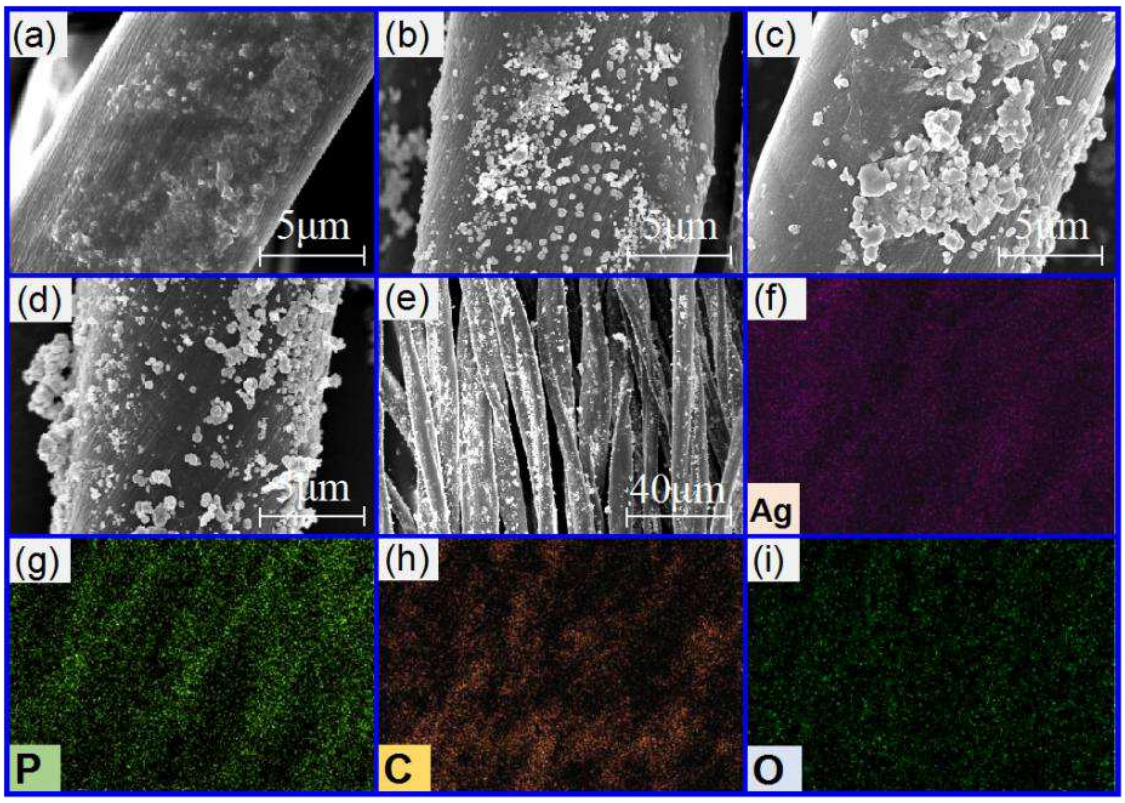

Fig. 4 SEM images of CA-Cotton (a), Ag_3PO_4@CA-Cotton with different Q_{SP} values (b: 50.4 mgg^{-1}, c: 173.6 mgg^{-1}, d: 345.9 mgg^{-1}, e: 50.4 mgg^{-1}) and corresponding EDX elemental mappings from (f-i)

CA-Cotton showed a relatively smooth surface (Fig. 4a) compared with Ag_3PO_4@CA-Cotton (Fig. 4b-d), which was responsible for the surface modification of CA molecules with cotton fiber (Li et al. 2015). A large number of Ag_3PO_4 particles were found on Ag_3PO_4@CA-Cotton, and the sizes of most particles were measured to be between 200 nm to 500 nm using Nano Measurer 1.2 software from SEM pictures. Specifically, some of these particles exhibited near-cubic appearance on the fiber in Fig. 4(c) and (d). Moreover, Fig. 4(e) provided a brief survey of Ag_3PO_4@CA-Cotton sample. It was clear that many cotton fibers were relatively evenly covered with Ag_3PO_4 particles without obvious gathering. The EDX elemental mapping of Ag_3PO_4@CA-Cotton was also presented in Fig. 4. Except for the two primary elements C and O, a small quantity of Ag and P elements were detected and observed to uniformly distribute on the surface of Ag_3PO_4@CA-Cotton. This demonstrated that Ag_3PO_4 were produced and deposited on CA-Cotton.

3.2.2 FTIR analysis

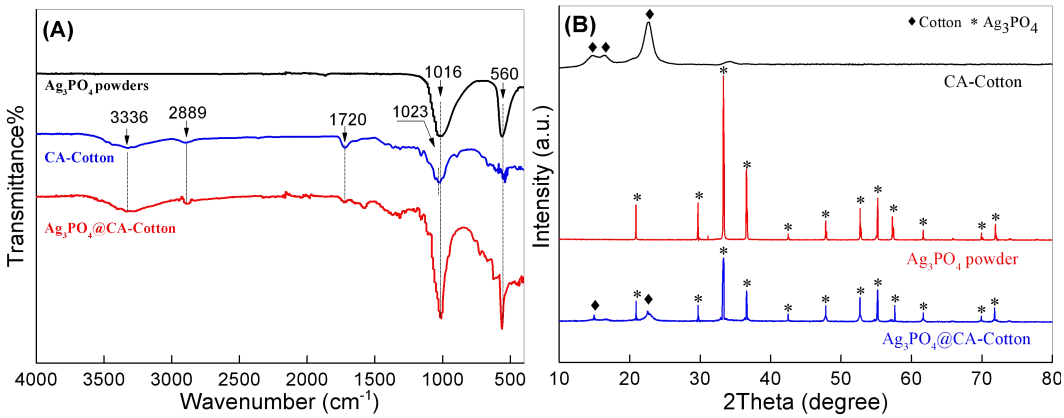

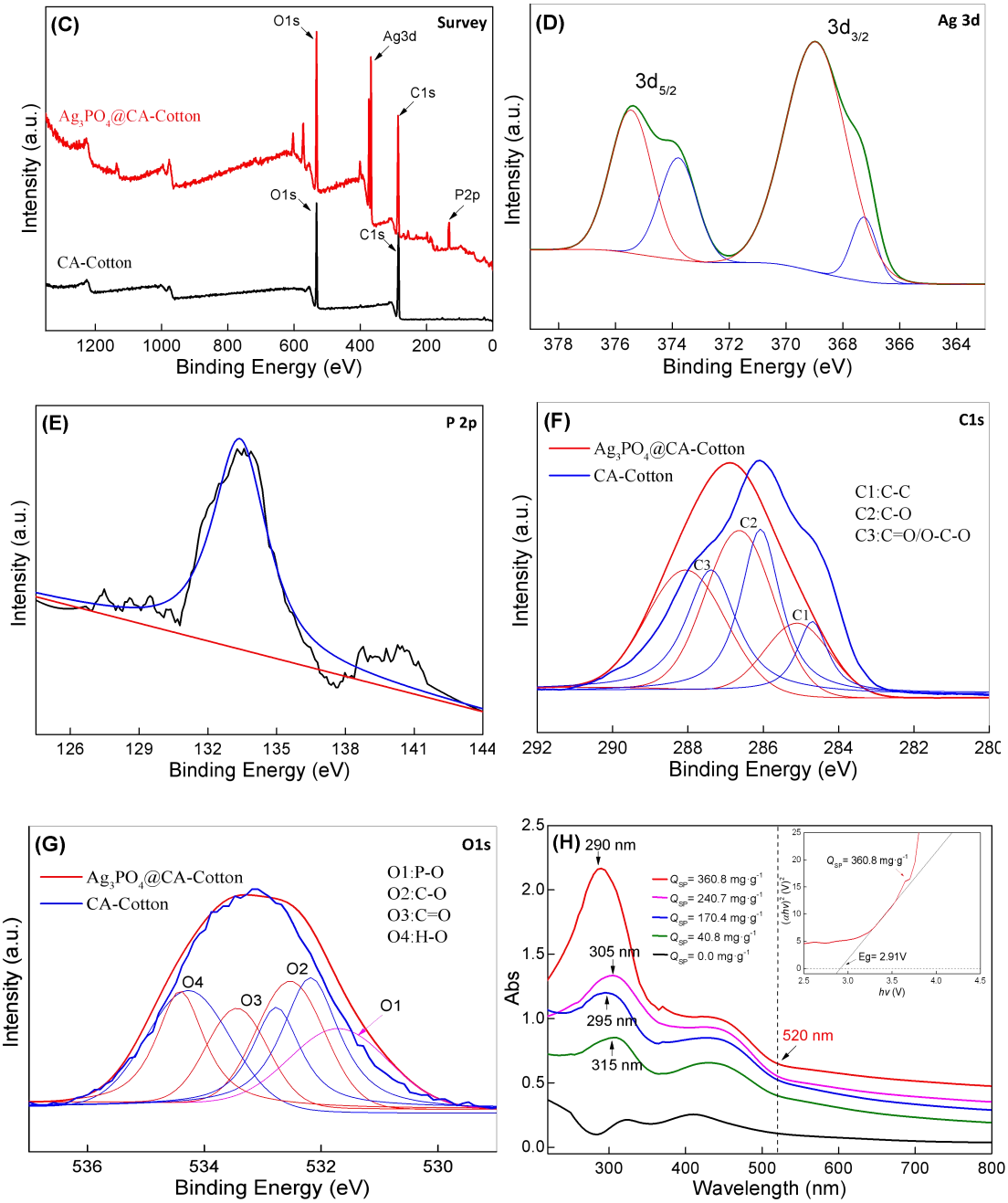

Fig. 5 FTIR (A), XRD (B), XPS (C-G) and UV-Vis-DRS (H) spectra of Ag_3PO_4@CA-Cotton

As shown in Fig. 5(A), both characteristic bands centered at 1016 and 560 cm^{-1} were found in the FTIR spectrum of pure Ag_3PO_4 particles, which were corresponded to the P-O bond vibration of the phosphate (PO_4^{3-}) (Dong et al. 2013; Xiong et al. 2018). Apart from several major peaks of the original cotton fiber including 3,340, 2,900, 1,431, 1,316, 1,158, 1,061, 1,033 and 905 cm^{-1} owing to the stretching of OH, CH, CO and C-O-C, a peak at 1720 cm^{-1} representing carbonyl stretching

vibration of the carboxyl groups (Li et al. 2015) was obviously observed in the FTIR spectrum of CA-Cotton. Comparatively, there were the main characteristic peaks of both Ag_3PO_4 and CA-Cotton in the spectrum of Ag_3PO_4@CA-Cotton. More importantly, it was obvious that the peak at 1720 cm^{-1} was less intensive in this spectrum. These revealed that Ag_3PO_4 particles were attached to CA-Cotton via the coordination between Ag^+ ion and carboxyl group.

3.2.3 XRD analysis

Fig. 5(B) displays the XRD spectra of CA-Cotton with three characteristic peaks at 14.50°, 16.72° and 22.81°, which were consistent with those reported in our previous study (Li et al. 2015). Besides, ten main peaks including 20.93°, 29.72°, 33.35°, 36.63°, 47.84°, 52.73°, 55.07°, 57.32°, 61.68°, and 71.95° were found from the spectra of pure Ag_3PO_4 particles, and they were attributed with the crystal planes of (110), (200), (210), (211), (310), (222), (320), (321), (400), and (421) of body-centered cubic phase Ag_3PO_4 (JCPDS card No. 06-0505), correspondingly (Song et al. 2018; Wang et al. 2013; Yan et al. 2013). Compared with CA-Cotton and Ag_3PO_4, Ag_3PO_4@CA-Cotton exhibited all the characteristic peaks of the two in its XRD spectra, indicating the existence of Ag_3PO_4 on CA-Cotton.

3.2.4 XPS analysis

To further confirm cotton fabric had been finished by Ag_3PO_4, Ag_3PO_4@CA-Cotton was investigated by using XPS technology, and the results were displayed in Fig. 5(C-G). Only the two peaks of C and O elements were detected in the XPS survey spectrum of CA-Cotton. With the exception of both peaks, another two peaks including Ag and P elements were also observed in the XPS survey spectrum of Ag_3PO_4@CA-Cotton. Moreover, there were two peaks at 375.6 eV ($Ag3d_{5/2}$) and 369.4 eV ($Ag3d_{3/2}$) in the Ag XPS spectrum. Both binding energies were slightly higher than

those (367.9 eV and 373.9 eV) of Ag^+ ions in pure Ag_3PO_4 (Djokovic et al. 2009; Yan et al. 2013). This was possibly because Ag^+ ions coordinated with carbonxyl groups on CA-Cotton. Additionally, the binding energy of O1s and C1s in Ag_3PO_4@CA-Cotton had an increment of 1.10 eV and 2.60 eV compared with CA-Cotton, respectively. It was also found that Ag_3PO_4@CA-Cotton showed three subpeaks C1 (C–C), C2 (C–O) and C3(C=O and O–C–O) (Li et al. 2015) with higher binding energies than those for CA-Cotton from the high-resolution carbon C1s spectrum. This further indicated the possible coordination of Ag^+ ions with carbonxyl groups. A P2p peak with 132.5 eV in Fig. 5(E) was corresponding to the P in PO_4^{3-} (Wang et al. 2013). O1s peak at 530.6 eV in Fig. 5(G) was from P–O of Ag_3PO_4 (Liu et al. 2014; Wang et al. 2013). These suggested that Ag_3PO_4 had been successfully deposited on CA-Cotton.

3.2.5 DRS analysis

Fig. 5(H) presented the DRS spectrum of CA-Cotton before and after Ag_3PO_4 finishing. It was clearly found that CA-Cotton had a very weak adsorption especially in UV range (<400 nm). By comparison, CA-Cotton showed both adsorption peaks located in 245-365 nm and 370-535 nm after Ag_3PO_4 finishing. Furthermore, increasing Q_{SP} value led to a gradual increment in the adsorption intensity of both peaks. This demonstrated that the prepared Ag_3PO_4@CA-Cotton possessed better light adsorption activity in UV and visible regions, which was mainly assigned to Ag_3PO_4 immobilized on CA-Cotton because pure Ag_3PO_4 usually provided an adsorption band edge around 530 nm (Yi et al. 2011). It was noteworthy that the adsorption band edge of Ag_3PO_4@CA-Cotton shifted above 550 nm, which was much more than 530 nm. This was similar to the phenomenons described when Ag_3PO_4 particles were combined with chitosan (Xiong et al. 2018) or acrylic polymer (Panthi et al. 2017) for preparing different composites. A possible reason was that the

ligand-to-metal charge transfer (LMCT) (Li et al. 2015) transitions from CA-Cotton toward Ag^+ ions in the complex produced with Ag^+ ions and carboxyl groups on CA-Cotton mentioned above in this study.

3.3 Photocatalytic evaluation

1.20 g of Ag_3PO_4@CA-Cotton (Q_{SP}=288.4 mgg^{-1}) was prepared through adjusting loading process. In order to enhance the stability of Ag_3PO_4 on cotton fabric, 0.04 $molL^{-1}$ KBr was added during the preparation, and the resulting Ag_3PO_4@CA-Cotton was then treated with 50 gL^{-1} fixing agent. The photocatalytic activity of Ag_3PO_4@CA-Cotton was evaluated by degrading azo dye RR 195 in aqueous solution with or without Ag_3PO_4@CA-Cotton under varied visible LED irradiation (LED-L: 1.87 $mWcm^{-2}$, LED-M: 5.10 $mWcm^{-2}$, LED-H: 14.95 $mWcm^{-2}$). *D*% values of RR 195 solutions were measured during the reaction and presented in Fig. 6(A).

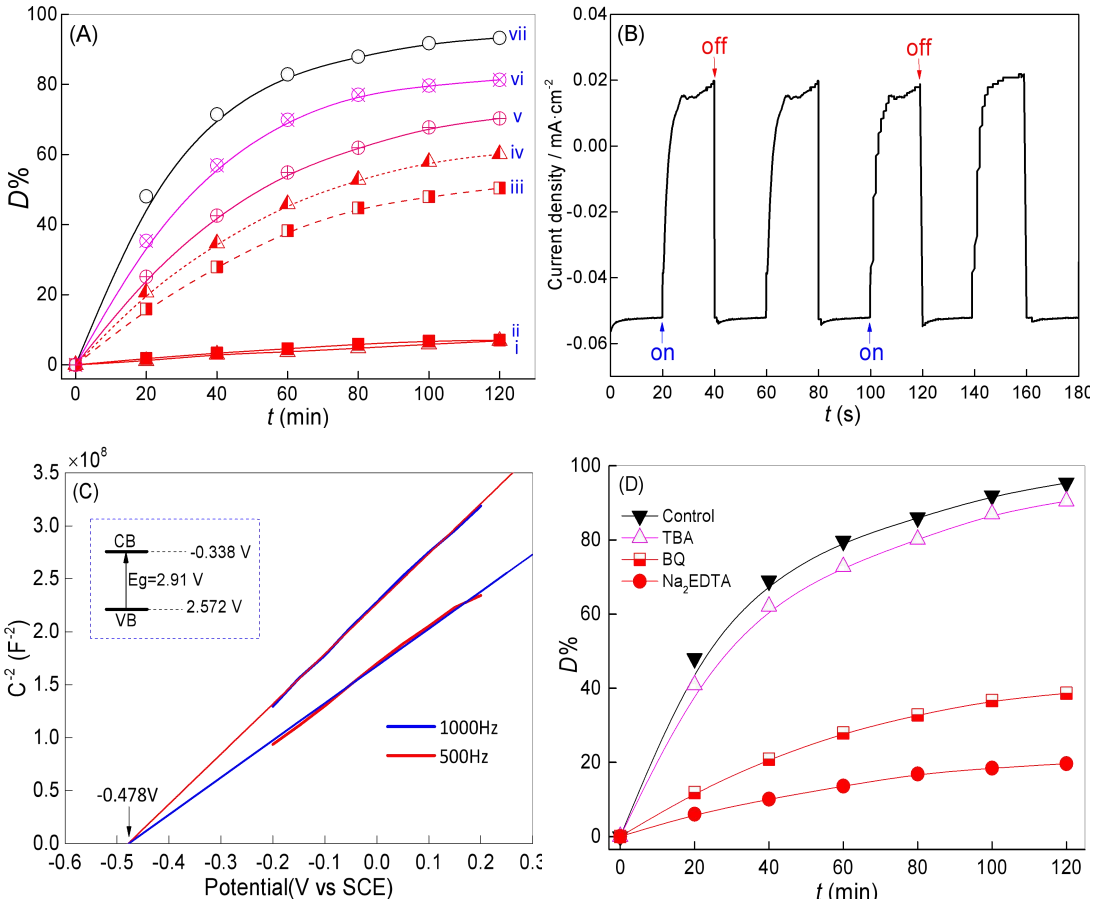

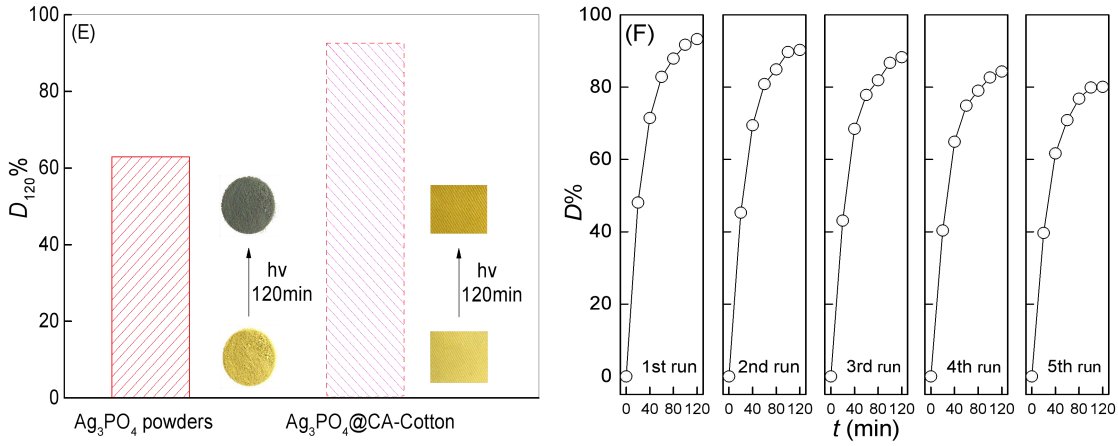

Fig. 6 Photocatalytic degradation of RR 195 in the presence of Ag_3PO_4@CA-Cotton at varied conditions(A), transient photocurrent response (B), Mott-Schottky plots of Ag_3PO_4@CA-Cotton (C), RR 195 degradation with or without different scavengers (D), anti-photocorrosion of Ag_3PO_4@CA-Cotton (E) and recycle runs of RR 195 degradation (F)

Fig. 6(A) showed that *D*% value slowly increased with CA-Cotton under LED-L irradiation, and *D*% value within 120min (D_{120}%) was 6.83% (curve i). D_{120}% was found to be 7.01% when Ag_3PO_4@CA-Cotton being used in the dark (curve ii). These results may be due to the weak adsorption of RR 195 molecules onto cotton fiber. In the case of Ag_3PO_4@CA-Cotton, once LED-L irradiation being introduced, *D*% value significantly increased up to 60.09% at the end of the reaction (curve v). Importantly, increasing LED irradiation intensity caused a gradual increment in *D*% value, and D_{120}% value was 80.32% or 93.28% under LED-M or LED-H irradiation, respectively (curves vi and vii). These finds confirmed that RR 195 could be effectively decomposed by Ag_3PO_4 as a photocatalyst on CA-Cotton under different visible LED irradiation, and high irradiation enhanced its photocatalytic degradation ability, thus accelerating RR 195 decomposition. By comparison, *D*% value for pure Ag_3PO_4 powders (curve iv) was less than that for Ag_3PO_4@CA-Cotton, demonstrating that Ag_3PO_4@CA-Cotton had better photocatalytic degradation capacity for RR 195 than Ag_3PO_4 powders at the same conditions. This may be mainly owing to the

complex between Ag^+ ions and CA-Cotton (named as Ag-CA-Cotton), which could serve as a bridge for the photo-electrons flowing from Ag_3PO_4 to CA-Cotton, thus favoring the subsequent free radical chain reaction through enhancing the transfer and separation of the photo-generated charge carriers at their interface (Liu et al. 2017; Shao et al. 2018). Besides, Ag-CA-Cotton was fabricated without Na_2HPO_4 by the same process, and then used as a substitute for Ag_3PO_4@CA-Cotton in this reaction. It was observed that D_{120}% value was 50.43% under LED-L irradiation (curve iii), which suggesting that Ag-CA-Cotton could photocatalyticaly oxidize RR 195 like a semiconductor. A possible reason may be that the abundance of metal nodes drove some coordination polymers to display semiconducting behavior when exposed to UV light or sunlight (Kulovi et al. 2017). Moreover, the blending of Ag(I) with suitable ligands can offer abroad variety of coordination geometry with a fair possibility of silver-silver interaction/bond formation (Bera et al. 2012a, b). Argentophilic interactions, occasionally ligand unsupported, in coordination polymers are important because they favor silver building block aggregation with concomitant brilliant photoluminescent behavior (Degtyarenko et al. 2008). These finds confirmed the superior photocatalytic performance of Ag_3PO_4@CA-Cotton as a novel hybrid photocatalyst.

Fig. 6(B) showed a stable and strong short circuit photocurrent response of the Ag_3PO_4 particles from CA-Cotton under several on-off visible light irradiation (14.95 $mWcm^{-2}$) cycles. It was clearly seen that this system was prompt in producing photocurrent with a reproducible response to on-off cycles, confirming better photogenerated electron and hole separation power of Ag_3PO_4@CA-Cotton. Moreover, a typical Mott-Schottky plot of Ag_3PO_4@CA-Cotton was tested in the dark at two different frequency of 500 and 1000 Hz, respectively, and presented in Fig. 6(C). Ag_3PO_4@CA-Cotton was found to be a *n*-type semiconductor owing to the positive slope of

Mott-Schottky plots (Araya et al. 2017; Gao et al. 2017). The intersection of the plots was independent of frequency. Subsequently, its flat-band potential was determined from Mott-Schottky plots was -0.478 V vs. SCE at pH 6.0, being equivalent to -0.238 V vs. NHE. The conduction band minimum (CBM) of Ag_3PO_4@CA-Cotton as a *n*-type semiconductor was negatively shifted to be -0.338 V versus NHE at pH 6.0 since the conduction band is 0-0.1 V lower than its flat band potential (Ai et al. 2014; Gao et al. 2017). Combined with the band gap energy estimated from UV-Vis DRS spectra shown in Fig. 4(D), the valence band (VB) potential of Ag_3PO_4 was calculated to be 2.572 V vs. NHE using an empirical formula: $E_{CB} = E_{VB} - E_g$ (Ai et al. 2014), which was higher than the redox potential of $\cdot OH/OH^-$ (2.38 V versus NHE) and thus indicating the possible formation of ·OH radicals. In general, redox potentials of organic dyes (Araya et al. 2017; Gao et al. 2017) are often significantly lower than VB potential of Ag_3PO_4, thus direct hole oxidation was thermodynamically permissible in the case of Ag_3PO_4@CA-Cotton under LED visible irradiation.

In order to study the role of active species generated in Ag_3PO_4@CA-Cotton/LED system, the photocatalytic decomposition of RR 195 was conducted with the existence of Ag_3PO_4@CA-Cotton and varied scavengers. It should be noticed that excess scavenger must be used in the experiments to ensure that all of the active species could be captured. According to literature (Amornpitoksuk and Suwanboon 2016; Yan et al. 2013), Na_2EDTA, 1,4-benzoquinone (BQ) and tertbutyl alcohol (TBA) were recommended as the scavengers for trapping photo-induced holes (H^+), superoxideradical ($\bullet O_2^-$) and hydroxyl radical (•OH), correspondingly. Thus, the tests were carried out by repeating RR 195 (0.02 $mmolL^{-1}$) degradation in the presence of Ag_3PO_4@CA-Cotton (288.4 mgg^{-1}) with the excessive addition of Na_2EDTA (0.30 $molL^{-1}$), BQ (0.02 $molL^{-1}$), or TBA (2.0 $molL^{-1}$), respectively. Meanwhile, blank test without any scavenger was also conducted at the same conditions, and *D*%

values were measured and provided in Fig. 6(D). In the blank test, *D*% value within 120 min (D_{120}%) reached 95.36% in the absence of scavenger. When TBA was introduced into the reaction process, the resulting *D*% curve was slightly lower than that in the blank test, and D_{120}% value was 92.35%, indicating that •OH had small contribution for RR 195 decomposition. More importantly, D_{120}% values were 38.64% and 19.66% with the addition of BQ and Na_2EDTA, correspondingly, proposing that photo-induced holes and $•O_2^-$ contributed 76.70% and 57.72% to dye decomposition. This proposed that photo-induced holes played a bigger role than $•O_2^-$ and •OH when Ag_3PO_4@CA-Cotton was used as photocatalyst. The contribution roles of three active species were similar to the results reported by Yan et al. (2013) and Amornpitoksuk et al. (2016). A main reason may be that both the highly dispersive valence bands and conduction bands of Ag_3PO_4 favor the transport of photoexcited electrons and holes (Ge et al. 2012). The photogenerated electrons could likely to react with H_2O and O_2 to produce $•O_2^-$, $•HO_2^-$ and •OH reactive oxygen species (ROS). Meanwhile, photogenerated holes would directly participate in the oxidation of pollutants. It is notable that direct hole oxidation is overmatched the traditional free radical oxidation (Li et al. 2015). In addition, PO_4^{3-} ions in Ag_3PO_4 have a large negative charge, which maintains a large dipole, thus promoting the separation of photogenerated electrons and holes through drawing holes and rejecting electrons for enhancing photocatalytic activity (Li et al. 2015). Moreover, several photostability tests were also performed to evaluate the anti-photocorrosion of Ag_3PO_4@CA-Cotton under LED-H irradiation. It was clear from Fig. 6(E) that D_{120}% values were 62.9% and 92.45% for pure Ag_3PO_4 powders and Ag_3PO_4@CA-Cotton, respectively. Simultaneously, pure Ag_3PO_4 powders were found to be turned dark gray after irradiating for 120 min. While color (yellow) of Ag_3PO_4@CA-Cotton was slightly changed within the same irradiating time, which supposed that Ag^+ ions on sample were

hardly reduced. Besides, Fig. 6(F) showed that increasing reuse of Ag_3PO_4@CA-Cotton led to an insignificant loss in *D*% value, and when it was reused five times, *D*% value was still higher than 80%. These results revealed that Ag_3PO_4@CA-Cotton not only limited the photocorrosion of Ag_3PO_4 through improving the movement of photogenerated electrons between Ag_3PO_4 and CA-Cotton, but also possessed good reuse ability in the photocatalytic degradation process due mainly to the coordination of Ag^+ ion with CA-Cotton and strong stabilizing power of fixing agent for Ag_3PO_4 on the fiber surface, thus which protected Ag_3PO_4 from dissolution and photocorrosion. However, the slight loss of photocatalytic ability during the recycles may result from the reason that a small number of Ag_3PO_4 particles would fall off from the fibers.

3.4 Self-cleaning capacity

Several Ag_3PO_4@CA-Cotton samples with different Q_{SP} levels were prepared and stained with 0.50 gL^{-1} of RR 195 aqueous solutions, respectively. And the stained samples were then irradiated in the photocatalytic self-cleaning test system. After irradiating for different times, all the samples were extracted with deionized water thoroughly, and the obtained solutions were examined using spectrometer. D_E% value were calculated for every sample during the tests and shown in Fig. 7(A).

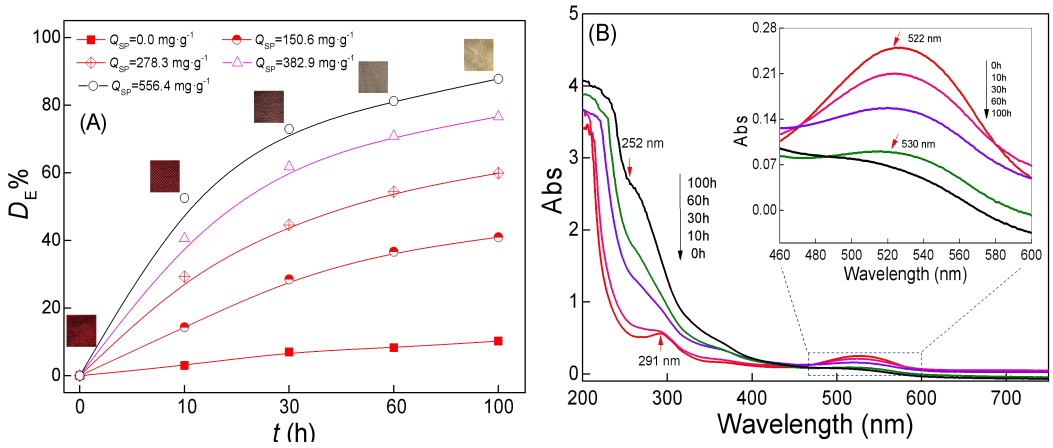

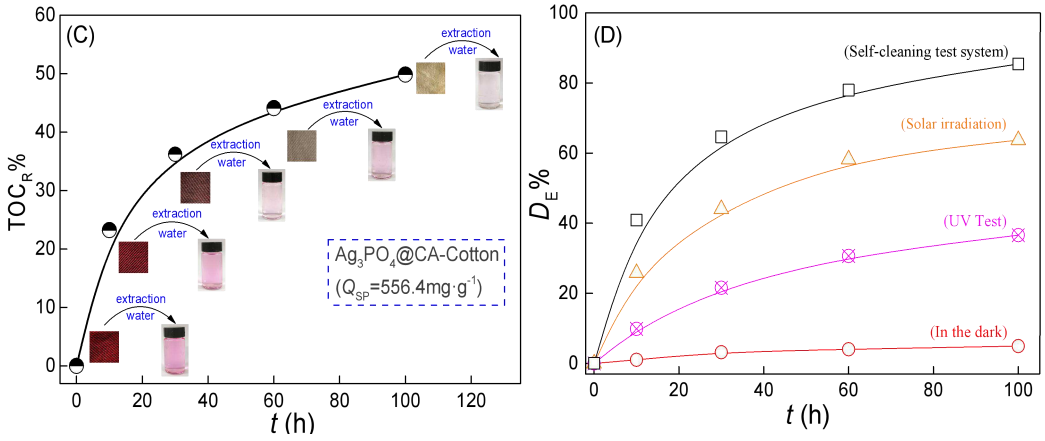

Fig. 7 Decomposition of RR 195 as a model stain on Ag_3PO_4@CA-Cotton during the self-cleaning procedure

Fig. 7(A) showed that D_E% value gradually increased with irradiation time. Increasing Q_{SP} levels caused a significant increment in D_E% value. This proposed that RR 195 molecules adsorbed could be destroyed by the oxidation of active species generated by Ag_3PO_4 on CA-Cotton, thus confirming that Ag_3PO_4@CA-Cotton exhibited effective self-cleaning capacity for RR 195, and high Q_{SP} level was crucial to achieve Ag_3PO_4 finished cotton fabric with high self-cleaning performance. It was clear from Fig. 7(B) that with the irradiation time from 0 to 100 h, a peak centered at 522 nm in the visible region became less intensive. Another peak at 291 nm in the UV region gradually shifted to 252 nm. These finds revealed that RR 195 molecules were broken into small aromatic compounds on the surface of fabric during the test. As shown in Fig. 7(C), TOC_R% value expressed the similar trend to D_E% value, and TOC_R% value was close to 50% after irradiating for 100 h, suggesting that some RR 195 molecules were converted into H_2O and CO_2 on the fiber, and the mineralization obviously increased during the reaction. Fig. 7(D) compared the decomposition profile of RR 195 with Ag_3PO_4@CA-Cotton exposured to different irradiation sources including UV light (0.13 $mWcm^{-2}$ at 340 nm) inside Fluorescent/UV Instrument (UV Test®), solar light (average intensity: 0.84 $mWcm^{-2}$ at 365 nm and 23.1 $mWcm^{-2}$ at 400-1000 nm) and high voltage halogen lamp (3.0 $mWcm^{-2}$ at 365nm

and 45.6 $mWcm^{-2}$ at 400-1000 nm) inside self-cleaning system. It was fact that D_E% value ranked as this order: self-cleaning system > solar light > UV Test, suggesting that self-cleaning system had much higher effectiveness to test Ag_3PO_4@CA-Cotton for the self-cleaning performance than solar light and UV Test system due to its strong irradiation power. On the other hand, Ag_3PO_4@CA-Cotton also showed relatively high self-cleaning performance under solar irradiation, which was of important significance for the future practical application of Ag_3PO_4@CA-Cotton as the self-cleaning material. To further study the degradation path of RR 195 on the surface of Ag_3PO_4@CA-Cotton, the extract liquids after irradiating for 100 h were examined by GC-MC to detect the intermediates generated from RR 195 during the irradiation process, and twelve possible intermediates were identified. Accordingly, a probable pathway of RR 195 decomposition on Ag_3PO_4@CA-Cotton was proposed in Fig. 8.

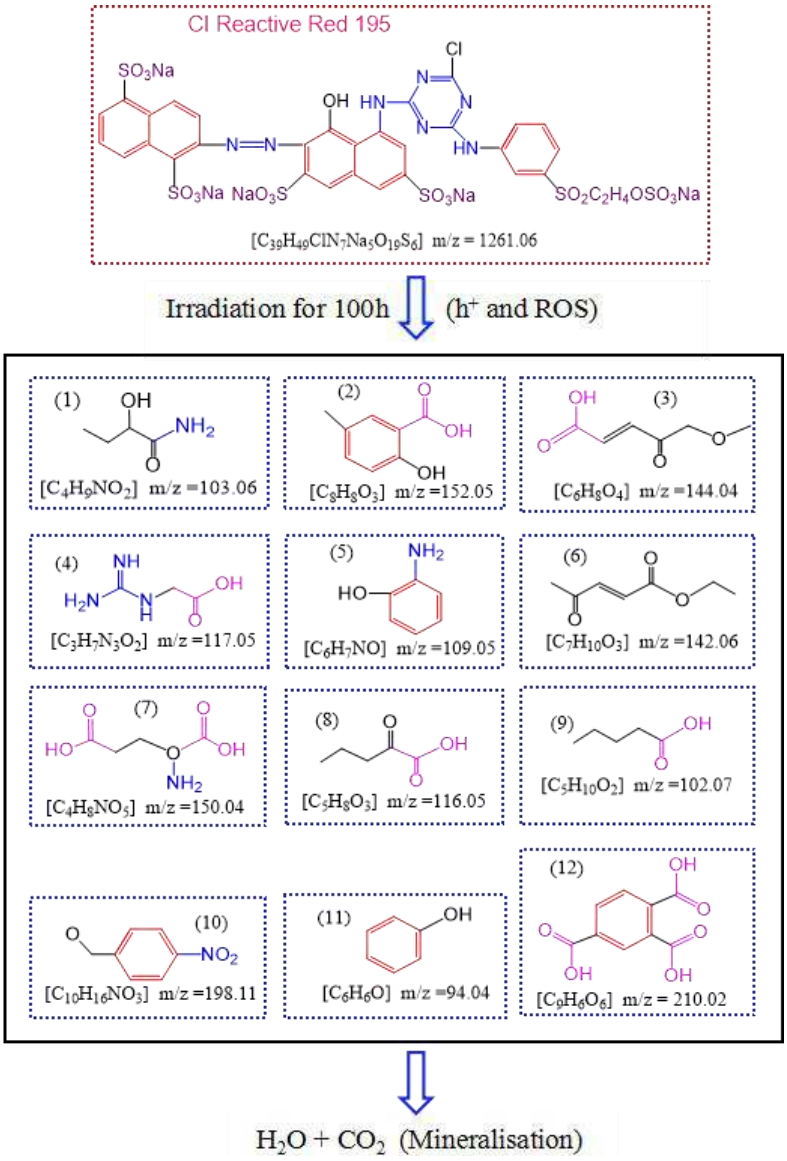

Fig. 8 A proposed degradation route of RR 195 on Ag_3PO_4@CA-Cotton surface during the self-cleaning process

Five intermediates were aromatic compounds (m/z=94-210), which may be produced by the destruction of the conjugated chromophore unit, especially splitting of the C-N= single bond and -N=N- bonds and subsequent ring opening of naphthalene in azo dye molecules (Bansal and Sud 2012; Hisaindee et al. 2013), due mainly to the oxidation of photogenerated holes and partly due to ROS (•OH and $•O_2^-$ radicals). This result was in good agreement with UV-Vis spectrum of RR 195 degradation process mentioned above. It should be stressed out that seven organic acids were

detected, and five of them were belong to liner fatty acids, which may be mainly formed by the direct oxidation of photogenerated holes and further transferred to CO_2 and H_2O (Guo et al. 2017). Moreover, the ring opening of cyclic hydrocarbon was dominated by the photogenerated holes (Liu et al. 2018). In addition, •OH and $•O_2^-$ radicals could attack and break C=C bonds in aromatic rings to convert them into carboxylic acids (Jin et al. 2019), thus causing their subsequent mineralization (Dong et al. 2019). These were responsible for gradually increasing TOC_R% value in Fig. 7(B).

4 Conclusions

Ag_3PO_4 particles could be effectively loaded on cotton fabric via CA cross-linking function using an industrialized pad-dry-cure finishing process. Surface carboxylation of cotton fabric with CA was a key step to prepare the Ag_3PO_4 finished cotton fabric (Ag_3PO_4@CA-Cotton) because Ag^+ ions could coordinate with the carboxyl groups on surface of cotton fabric, and further reacted with PO_4^{3-} ions in order to obtain Ag_3PO_4 particles. High Q_{COOH} value dramatically increased Q_{SP} and L_{SP}% values of Ag_3PO_4@CA-Cotton. It should be emphasized that the industrialized pad-dry-cure process could more strongly fix Ag_3PO_4 particles on cotton fabric than the conventional dipping method since padding roller pressure significantly enhanced the reaction between Ag^+, PO_4^{3-} ions and carboxyl groups on cotton fabric. Ag_3PO_4@CA-Cotton showed stronger photocatalytic capacity than pure Ag_3PO_4 particles owing to the synergetic effect of the Ag complex with the carboxyl groups on cotton fabric. Moreover, the addition of KBr and fixing agent further improved the loading of Ag_3PO_4 particles on cotton fabric and the stability of the resulting Ag_3PO_4@CA-Cotton. Besides, Ag_3PO_4@CA-Cotton exhibited better self-cleaning performance for the model dye stain under varied irradiation. The dye was found to be almost completely decomposed and partly mineralized on Ag_3PO_4@CA-Cotton after the irradiating for 100h using a homemade self-cleaning test system.

Overall, the experimental finds illustrated that the combination of CA cross-linking function and Ag^+ ion coordination was considered as a necessary strategy to finish cotton fabric with Ag_3PO_4 using the industrialized padding process, thus favoring the practical application of Ag_3PO_4 photocatalyst in the day to come.

Acknowledgement

This research was supported by Innovation & Pioneering Talents Plan of Jiangsu Province (2015-340).

References

Ai L, Zhang C, Li L, Jiang J (2014) Iron terephthalate metal-organic framework: Revealing the effective activation of hydrogen peroxide for the degradation of organic dye under visible light irradiation. Appl Catal B-Environ 148:191-200.

Amornpitoksuk P, Suwanboon S (2016) Photocatalytic degradation of dyes by AgBr/Ag_3PO_4 and the ecotoxicities of their degraded products. Chinese J Catal 37:711-719.

Araya T, Jia M, Yang J, Zhao P, Cai K, Ma W, Huang Y (2017) Resin modified MIL-53(Fe) MOF for improvement of photocatalytic performance. Appl Catal B-Environ 203:768-777.

Bansal P, Sud D (2012) Photodegradation of commercial dye CI Reactive Blue 160 using ZnO nanopowder: Degradation pathway and identification of intermediates by GC/MS. Sep Purif Technol 85:112-119.

Bera M, Rana A, Chowdhuri D, Hazari D, Jana S, Puschmann H, Dalai S (2012a) A New 3D Silver(I) Coordination Polymer with Octadentate Diglycolate Ligand Having Silver-Silver Bond. J Inorg Organomet P 22:1074-1080.

Bera M, Rana A, Chowdhuri D, Hazari D, Jana S, Puschmann H, Dalai S (2012b)

Three-Dimensional Silver(I)-Thiodiglycolate Coordination Polymer with Weak Ag–Ag Bond. J Inorg Organomet P 22:897-902.

Bi Y, Ouyang S, Cao J, Ye J (2011) Facile synthesis of rhombic dodecahedral AgX/Ag_3PO_4 (X=Cl Br I) heterocrystals with enhanced photocatalytic properties and stabilities. Phys Chem Chem Phys 13(21):10071-10075.

Burunkaya E, Akarsu M, Camurlu HE, Kesmez O, Yesil Z, Asilturk M, Arpac E, (2013) Production of stable hydrosols of crystalline TiO_2 nanoparticles synthesized at relatively low temperatures in diverse media. Appl Surf Sci 265:317-323.

Cai L, Long Q, Yin C (2014) Synthesis and characterization of high photocatalytic activity and stable Ag_3PO_4/TiO_2 fibers for photocatalytic degradation of black liquor. Appl Surf Sci 319(1) :60-67.

Chen P, Zhang L, Wu Q, Yao W (2016) Novel synthesis of Ag_3PO_4/CNFs/silica-fiber hybrid composite as an efficient photocatalyst. J Taiwan Inst Chem E 63:506-511.

Curran J, Sc B (2009) Silver (I) complexes as antimicrobial and anticancer drugs. Soc Psych 42(2):135-143.

Degtyarenko AS, Solntsev PV, Krautscheid H, Rusanov EB, Chernega AN, Domasevitch KV (2008) Copper(I) and silver(I) coordination frameworks involving extended bipyridazine bridges. New J Chem 32(11):1910-1918.

Djokovic V, Krsmanovic R, Bozanic D, McPherson M, Tendeloo G, Nair P, Georges M, Radhakrishnan T (2009) Adsorption of sulfur onto a surface of silver nanoparticles stabilized with sago starch biopolymer. Colloid Surface B 73(1):30-35.

Dong P, Wang Y, Cao B, Xin S, Guo L, Zhang J, Li F (2013) Ag_3PO_4/reduced graphite oxide sheets nanocomposites with highly enhanced visible light photocatalytic activity and stability. Appl

Catal B-Environ 132-133:45-53.

Dong Y, Han Z, Liu C, Du F (2010) Preparation and photocatalytic performance of Fe(III)-amidoximated PAN fiber complex for oxidative degradation of azo dye under visible light irradiation. Sci Total Environ 408(10):2245-2253.

Dong Y, Wang P, Li B (2019) Fe complex immobilized on waste polypropylene fibers for fast degradation of Reactive Red 195 via enhanced activation of persulfate under LED visible irradiation. J Clean Prod 208:1347-1356.

Gao Y, Li S, Li Y, Yao L, Zhang H (2017) Accelerated photocatalytic degradation of organic pollutant over metal-organic framework MIL-53(Fe) under visible LED light mediated by persulfate. Appl Catal B-Environ 202:165-174.

Ge M, Zhu N, Zhao Y, Li J, Liu L (2012) Sunlight-Assisted Degradation of Dye Pollutants in Ag_3PO_4 Suspension. Ind Eng Chem Res 51(14):5167-5173.

Guo J, Dai Y, Chen X, Zhou L, Liu T (2017) Synthesis and characterization of $Ag_3PO_4/LaCoO_3$ nanocomposite with superior mineralization potential for bisphenol A degradation under visible light. J Alloy Compo 696(5):226-233.

Guo Y, Yu W, Chen J, Wang X, Gao B, Wang G (2017) Ag_3PO_4/rectorite nanocomposites: Ultrasound-assisted preparation characterization and enhancement of stability and visible-light photocatalytic activity. Ultrason Sonochem 34:831-838.

Hisaindee S, Meetani MA, Rauf MA (2013) Application of LC-MS to the analysis of advanced oxidation process (AOP) degradation of dye products and reaction mechanisms. Trend Anal Chem 49:31-44.

Ji Y, Lin K, Zheng H, Liu C, Dudik L, Zhu J, Burda C (2010) Solar-light photoamperometric and

photocatalytic properties of quasi-transparent TiO_2 nano porous thin films. ACS Appl Mater Inter 2(11):3075-3082.

Jiang X, Chen C, Chen W, Yu A (2010) Role of citric acid in the formation of silver nanoplates through a synergistic reduction approach. Langmuir 26(6):4400-4408.

Jiao Z, Zhang Y, Yu H, Lu G, Ye J, Bi Y (2012) Concave trisoctahedral Ag_3PO_4 microcrystals with high-index facets and enhanced photocatalytic properties. Chem Commun 49(6):636-638.

Jin J, Liu M, Feng L, Wang H, Wang Y, Nguyen TAH, Wang Y, Lu J, Li Y, Bao M (2019) 3D Bombax-structured carbon nanotube sponge coupling with Ag_3PO_4 for tetracycline degradation under ultrasound and visible light irradiation. Sci Total Environ 695:133694.

Kamegawa T, Suzuki N, Yamashita H (2011) Design of acroporous TiO_2 thin film photocatalysts with enhanced photofunctional properties. Energ Environ Sci 4 (4):1411-1416.

Kulovi S, Das S, Zangrando E, Puschmann H, Dalai S (2017) New Silver(I) Coordination Polymers with Hetero Donor Ligands: Synthesis Structure Luminescence Study and Photo-Catalytic Behavior. Chemistry Select 2:9029-9036.

Li B, Dong Y, Li L (2015) Preparation and catalytic performance of Fe(III)-citric acid-modified cotton fiber complex as a novel cellulose fiber-supported heterogeneous photo-Fenton catalyst. Cellulose 22(2):1295-1309.

Li X, Xu P, Chen M, Zeng G, Wang D, Chen F, Tang W, Chen C, Zhang C, Tan X (2019) Application of silver phosphate-based photocatalysts: Barriers and solutions. Chem Eng J 366:339-357.

Li Y, Zhou H, Zhu G, Shao C, Pan H, Xu X, Tang R (2015) High efficient multifunctional Ag_3PO_4 loaded hydroxyapatite nanowires for water treatment. J Hazard Mater 299:379-387.

Lin Y, Hsu Y, Chen Y, Wang S, Miller J, Chen L, Chen K (2012) Plasmonic $Ag@Ag_3(PO_4)_{1-x}$

nanoparticle photosensitized ZnO nanorod-array photoanodes for water oxidation. Energ Environ Sci 5(2):8917-8922.

Liu J, Wang Y, Wang Y, Fan C (2014) Synthesis regeneration and photocatalyticactivity under visible-light irradiation of $Ag/Ag_3PO_4/g\text{-}C_3N_4$ hybrid photocatalysts. Acta Phys Chim Sin 30(4):729-737.

Liu L, Ding L, Liu Y, An W, Lin S, Liang Y, Cui W (2017) A stable Ag_3PO_4@PANI core@shell hybrid: Enrichment photocatalytic degradation with π-π conjugation. Appl Catal B-Environ 201:92-104.

Liu Y, Kong J, Yuan J, Zhao W, Zhu X, Sun C, Xie J (2018) Enhanced photocatalytic activity over flower-like sphere $Ag/Ag_2CO_3/BiVO_4$ plasmonic heterojunction photocatalyst for tetracycline degradation. Chem Eng J 331:242-254.

Lucas M, Tavares P, Peres J, Faria J, Rocha M, Pereira C, Freire C (2013) Photocatalytic degradation of Reactive Black 5 with TiO_2-coated magnetic nanoparticles. Catal Today 209:116-121.

Panthi G, Park SJ, Chae SH, Kim TW, Chung HJ, Hong ST, Park M, Kim HY (2017) Immobilization of Ag_3PO_4 nanoparticles on electrospun PAN nanofibers via surface oximation: Bifunctional composite membrane with enhanced photocatalytic and antimicrobial activities. J Ind Eng Chem 45:277-286.

Pasta M, Mantia F, Hu L, Deshazer H, Cui Y (2010) Aqueous supercapacitors on conductive cotton. Nano Res 3(6):452-458.

Shao N, Hou Z, Zhu H, Wang J, Francois-Xavier C (2018) Novel 3D core-shell structured $CQDs/Ag_3PO_4$@Benzoxazine tetrapods for enhancement of visible-light photocatalytic activity and anti-photocorrosion. Appl Catal B-Environ 232:574-586.

Shen W, Dong Y, Cui G, Li B (2016) Optimized preparation of electrically conductive cotton fabric by an industrialized exhaustion dyeing with reduced graphene oxide. Cellulose 23(5):3291-3300.

Song L, Li T, Zhang S (2018) Preparation of high ctivity AgBr/Ag_3PO_4 photocatalyst based on hexadecyltrimethylammonium bromide and mechanism of photocatalytic enhancement. Appl Organomet Chem 32(3):4209-4215.

Wang J, Wang P, Cao Y, Chen J, Li W, Shao Y, Zheng Y, Li D (2013) A high efficient photocatalyst Ag_3VO_4/TiO_2/graphene nanocomposite with wide spectral response. Appl Catal B-Environ 136:94-102.

Wang P, Dong Y, Li B, Li Z, Bian L (2018) A sustainable and cost effective surface functionalization of cotton fabric using TiO_2 hydrosol produced in a pilot scale: Condition optimization sunlight-driven photocatalytic activity and practical applications. Ind Crop Prod 123:197-207.

Wang Q, Cai J, Zhang L (2014) In situ synthesis of Ag_3PO_4/cellulose nanocomposites with photocatalytic activities under sunlight. Cellulose 21(5):3371-3382.

Wang Y, Li X, Wang Y, Fan C (2013) Novel visible-light AgBr/Ag_3PO_4 hybrids photocatalysts with surface plasma resonance effects. J Solid State Chem 202:51-56.

Whitcomb D, Rajeswaran M (2006) Designing silver carboxylate polymers: Crystal structures of silver-acetyl-benzoate and silver-12-benzenedicarboxylate monomethyl ester. Polyhedron 25(8):1747-1752.

Xiong S, Liu M, Yan J, Zhao Z, Wang H, Yin X, Wang L, Chen S (2018) Immobilization of Ag_3PO_4 nanoparticles on chitosan fiber for photocatalytic degradation of methyl orange. Cellulose 25(9):5007-5015.

Yan X, Gao Q, Qin J, Yang X, Li Y, Tang H (2013) Morphology-controlled synthesis of Ag_3PO_4 microcubes with enhanced visible-light-driven photocatalytic activity. Ceram Int 39(8):9715-9720.

Yang Z, Huang G, Huang W, Wei J, Yan X, Liu Y, Jiao C, Wan Z, Pan A (2013) Novel Ag_3PO_4/CeO_2 composite with high efficiency and stability for photocatalytic applications. J Mater Chem A 2(6):1750-1756.

Yao W, Zhang B, Huang C, Ma C, Song X, Xu Q (2012) Synthesis and characterization of high efficiency and stable Ag_3PO_4/TiO_2 visible light photocatalyst for the degradation of methylene blue and rhodamine B solutions. J Mater Chem 22(9):4050-4055.

Yi Z, Ye J, Kikugawa N, Kako T, Ouyang S, Stuart-Williams H, Yang H, Cao J, Luo W, Li Z, Liu Y, Withers R (2010) An orthophosphate semiconductor with photooxidation properties under visible-light irradiation. Nat Mater 9(7):559-564.

Young A, Hanton L (2008) Square planar silver(I) complexes: A rare but increasingly observed stereochemistry for silver(I). Coordin Chem Rev 252(12-14):1346-1386.

Yu H, Jiao Z, Hu H, Lu G, Ye J, Bi Y (2013) Fabrication of Ag_3PO_4-PAN composite nanofibers for photocatalytic applications. CrystEngComm 15(24):4802-4805.

Yu L, He J, Huang C, Li M, Zhang Y, Zhou X, Zhu H (2017) Electron transportation path build for superior photoelectrochemical performance of Ag_3PO_4/TiO_2. RSC Adv 7:54485.

Zhu H, Zhang X, Liu X, Wang X, Liu G, Usman A, Fun H (2003) Clear Ag-Ag bonds in three silver(I) carboxylate complexes with high cytotoxicity properties. Inorg Chem Commun 6(8):1113-1116.

Figures

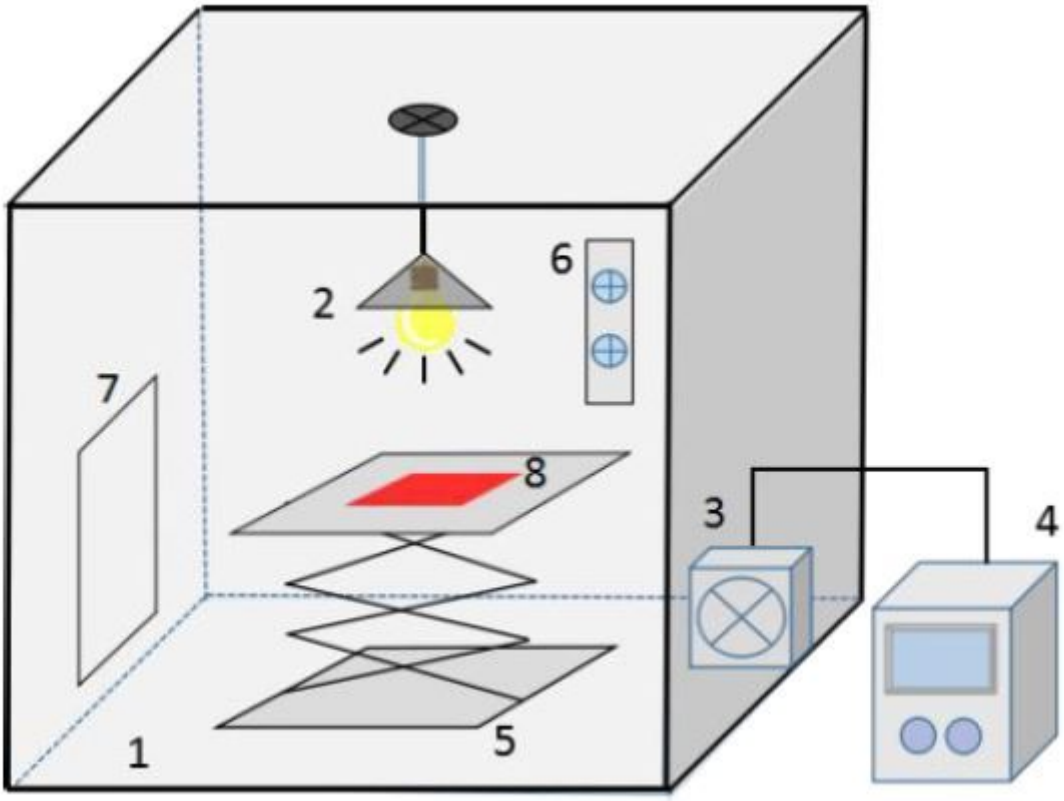

Figure 1

Diagrammatic sketch of photocatalytic self-cleaning test system: (1) test chamber, (2) high voltage halogen lamp, (3) circulation air fan, (4) temperature controller, (5) vertical lifting sample stage, (6) temperature and humidity indicator, (7) sampling gate, (8) test sample

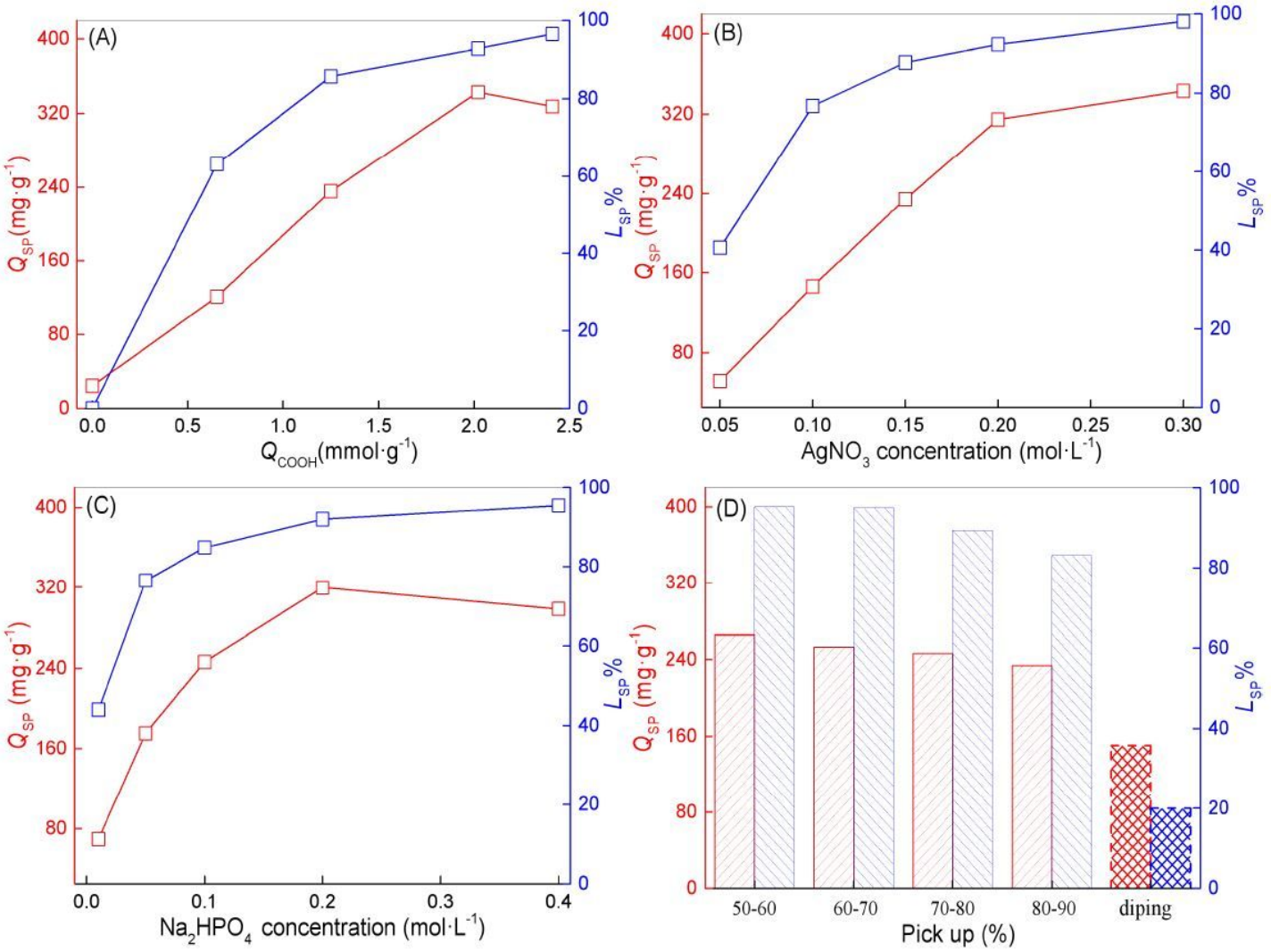

Figure 2

Effect of finishing process on QSP and LSP% values of Ag3PO4@CA-Cotton

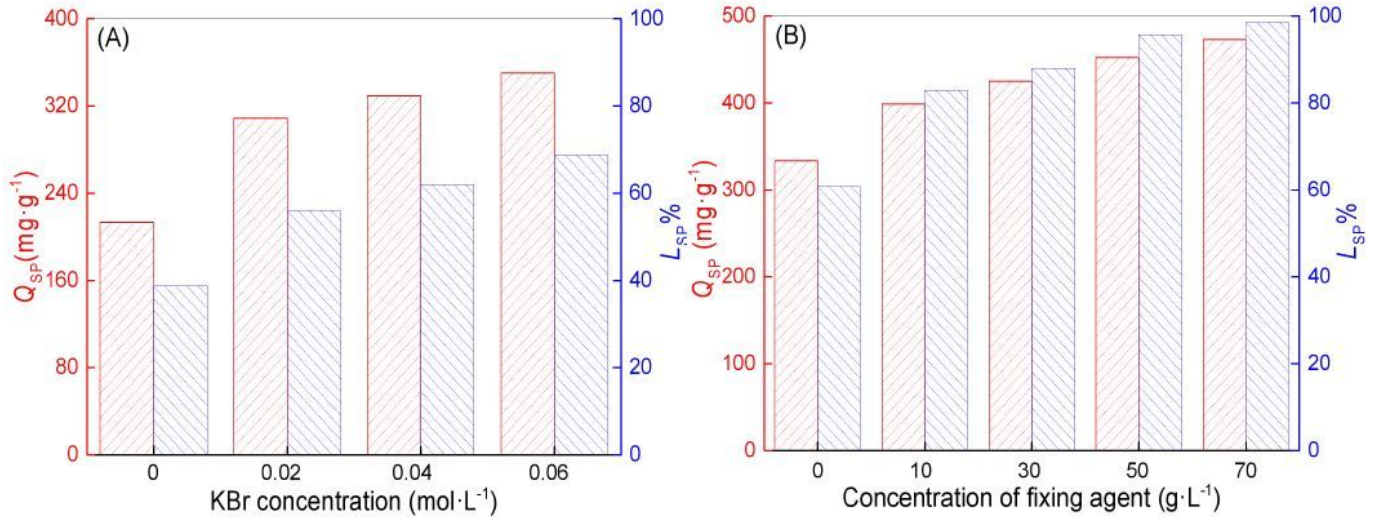

Figure 3

Enhanced effect of KBr (A) and fixing agent (B) on loading of Ag3PO4 on cotton fabric

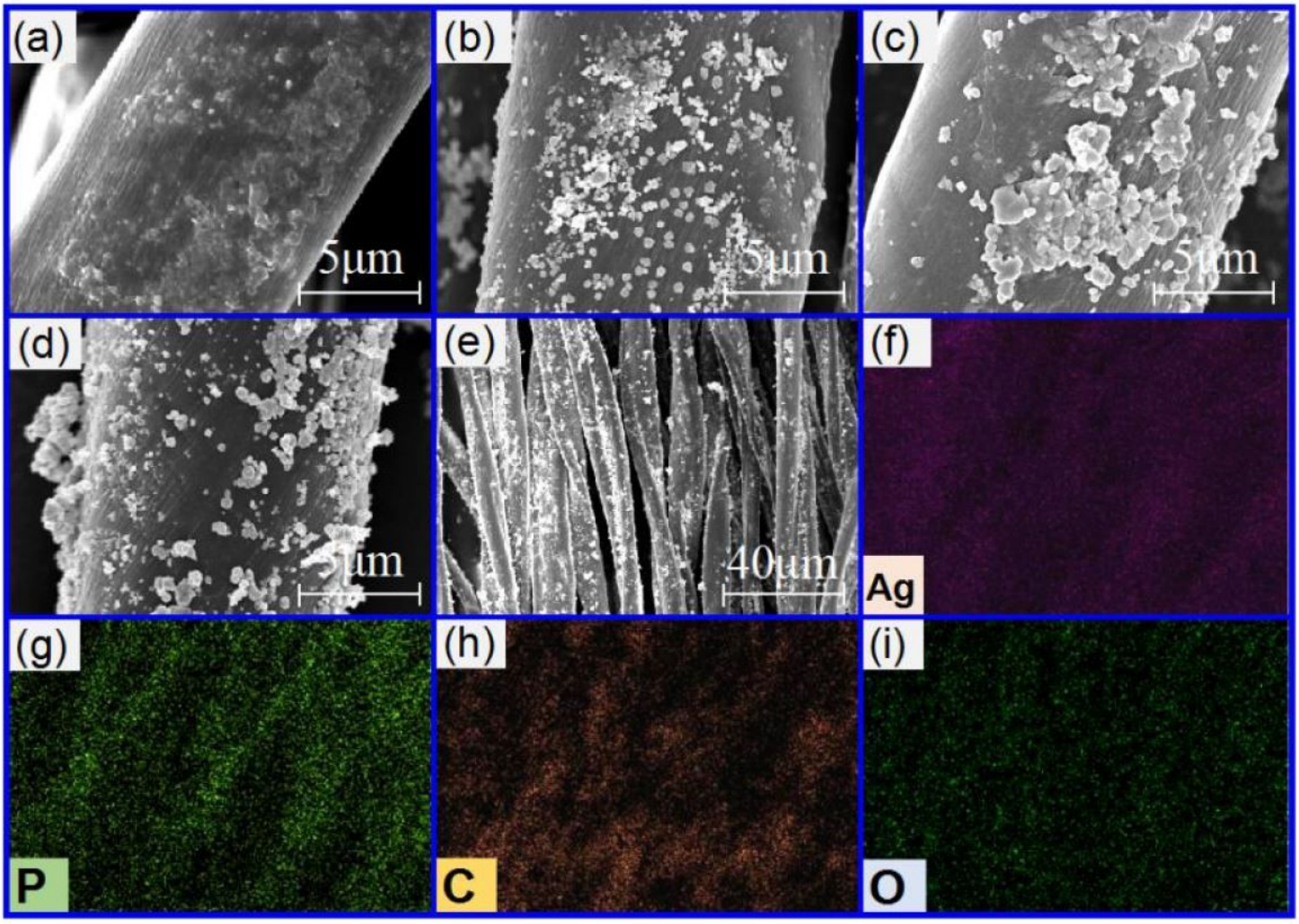

Figure 4

SEM images of CA-Cotton (a), Ag3PO4@CA-Cotton with different QSP values (b: 50.4 mgg-1, c: 173.6 mgg-1, d: 345.9 mgg-1, e: 50.4 mgg-1) and corresponding EDX elemental mappings from (f-i) CA-Cotton showed a relatively smooth surface (Fig. 4a) compared with Ag3PO4@CA-Cotton (Fig. 4b-d), which was responsible for the surface modification of CA molecules with cotton fiber (Li et al. 2015). A large number of Ag3PO4 particles were found on Ag3PO4@CA-Cotton, and the sizes of most particles were measured to be between 200 nm to 500 nm using Nano Measurer 1.2 software from SEM pictures. Specifically, some of these particles exhibited near-cubic appearance on the fiber in Fig. 4(c) and (d). Moreover, Fig. 4(e) provided a brief survey of Ag3PO4@CA-Cotton sample. It was clear that many cotton fibers were relatively evenly covered with Ag3PO4 particles without obvious gathering. The EDX elemental mapping of Ag3PO4@CA-Cotton was also presented in Fig. 4. Except for the two primary elements C and O, a small quantity of Ag and P elements were detected and observed to uniformly distribute on the surface of Ag3PO4@CA-Cotton. This demonstrated that Ag3PO4 were produced and deposited on CA-Cotton.

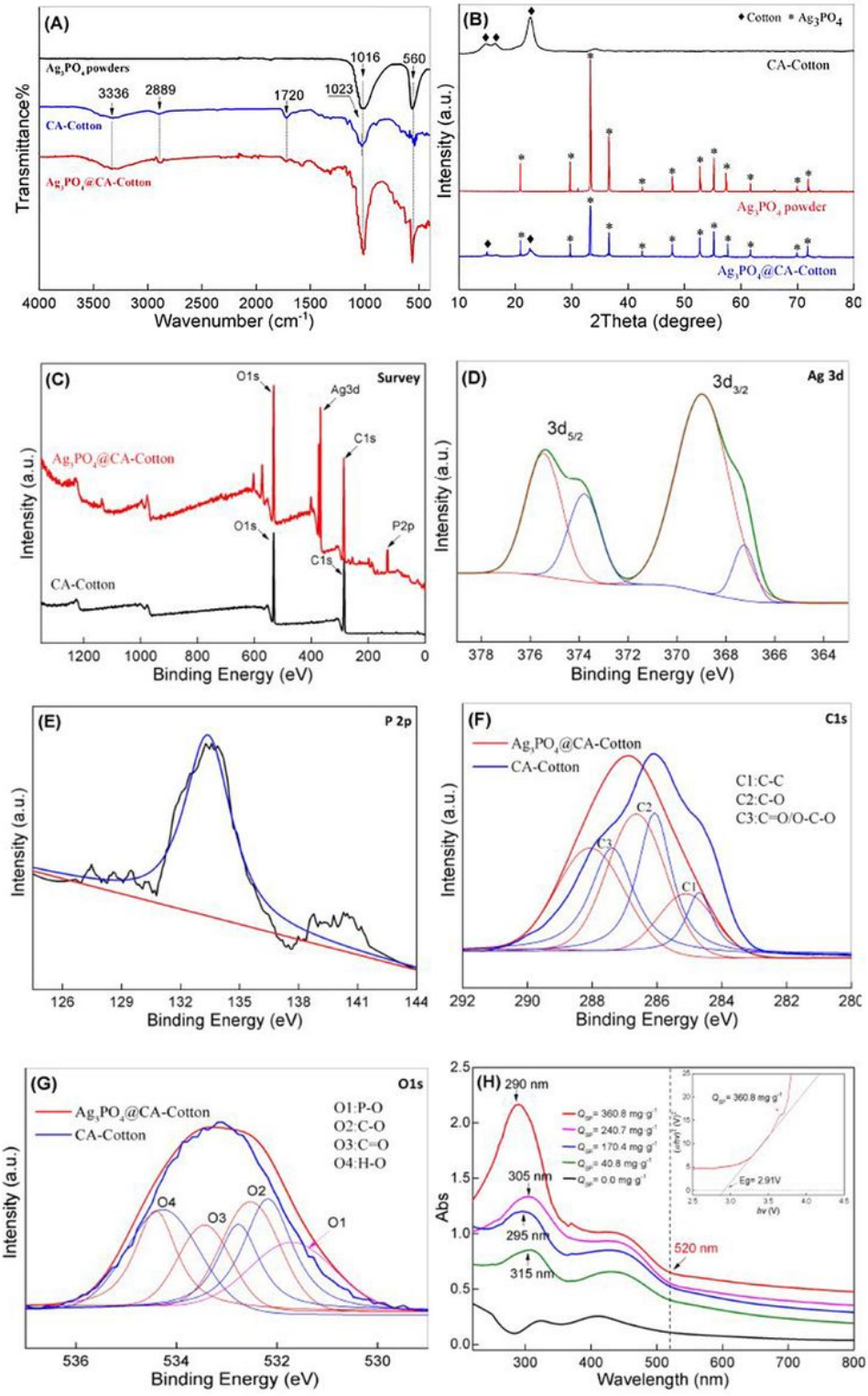

Figure 5

FTIR (A), XRD (B), XPS (C-G) and UV-Vis-DRS (H) spectra of Ag3PO4@CA-Cotton

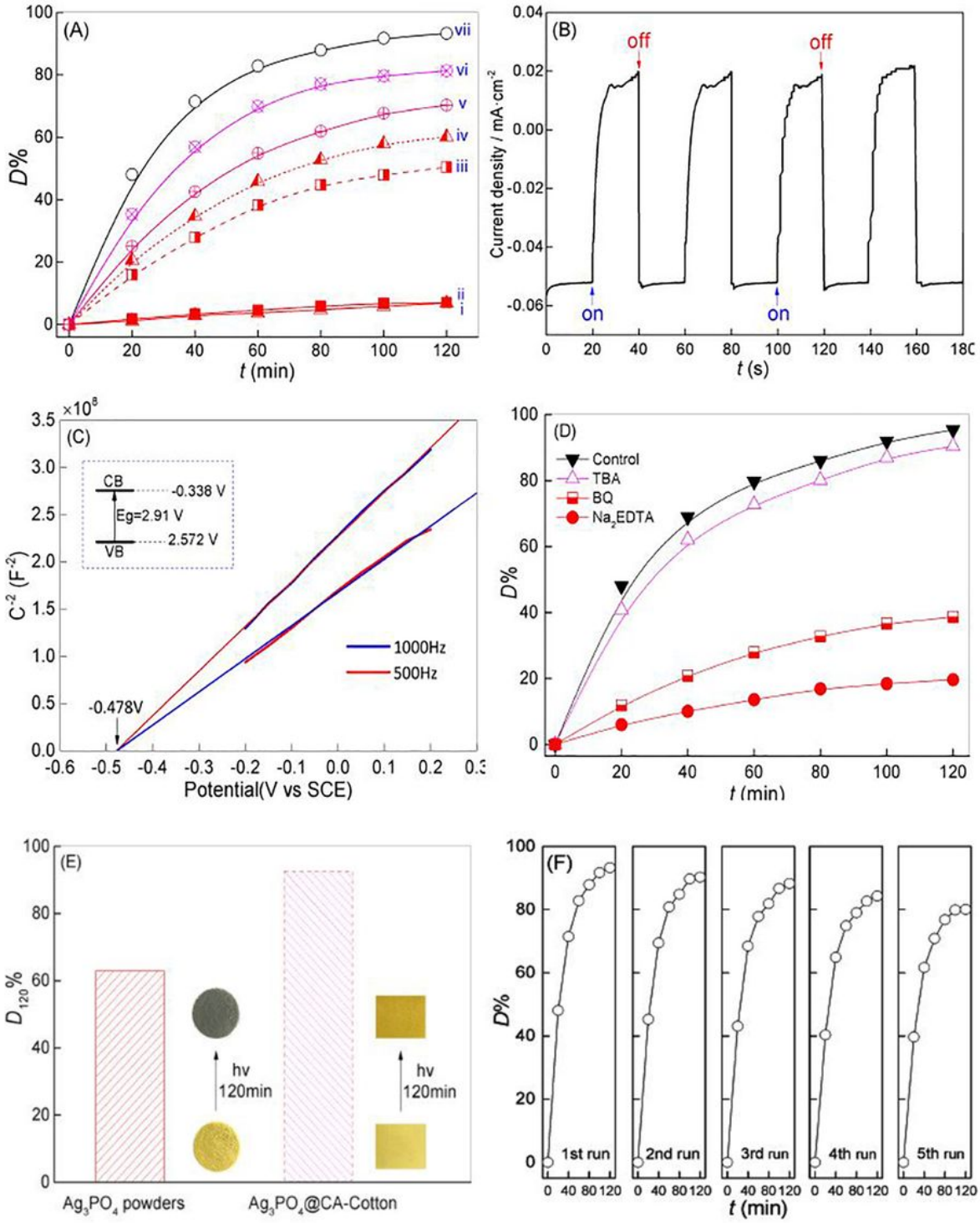

Figure 6

Photocatalytic degradation of RR 195 in the presence of Ag3PO4@CA-Cotton at varied conditions(A), transient photocurrent response (B), Mott-Schottky plots of Ag3PO4@CA-Cotton (C), RR 195 degradation with or without different scavengers (D), anti-photocorrosion of Ag3PO4@CA-Cotton (E) and recycle runs of RR 195 degradation (F)

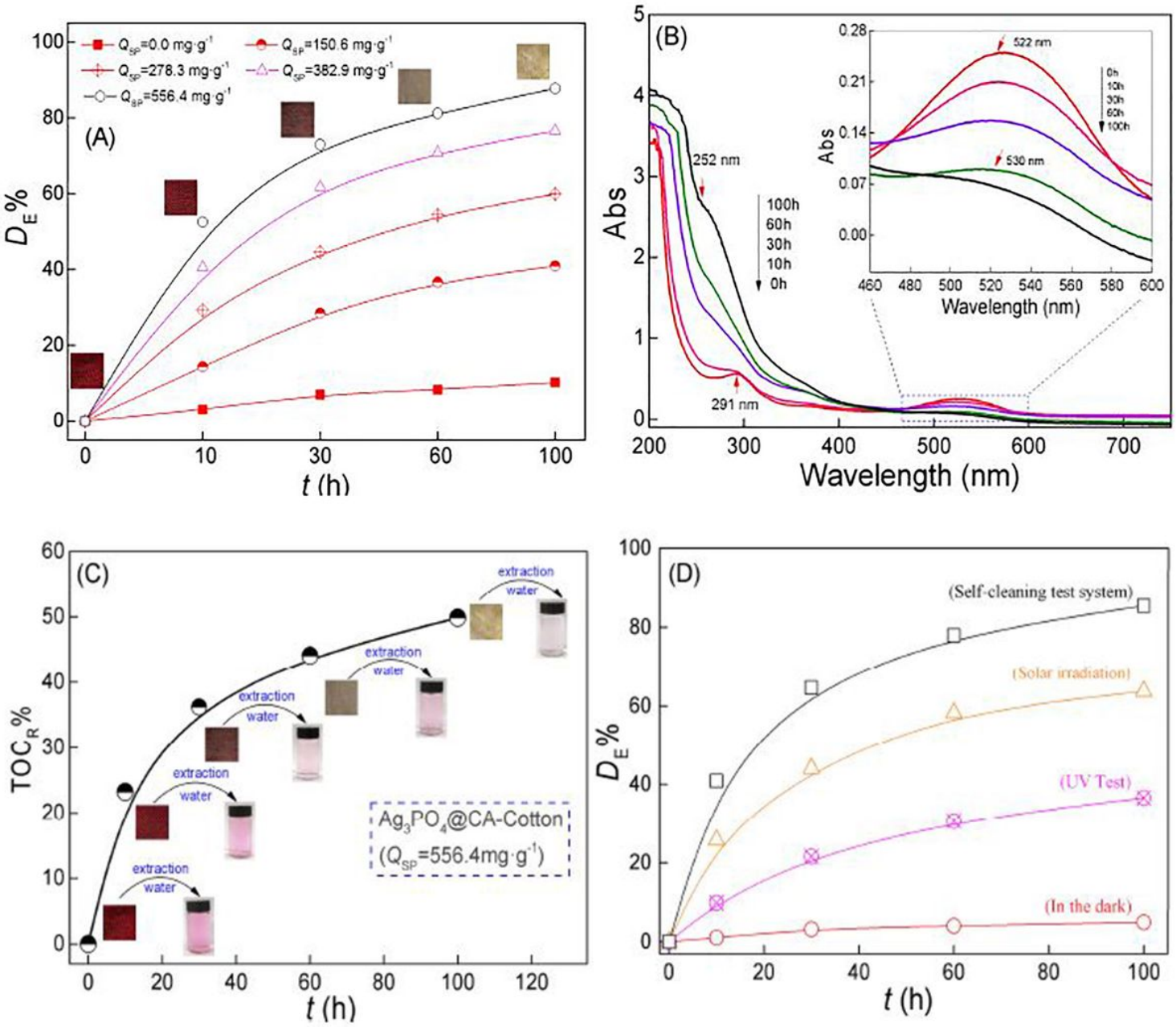

Figure 7

Decomposition of RR 195 as a model stain on Ag3PO4@CA-Cotton during the self-cleaning procedure

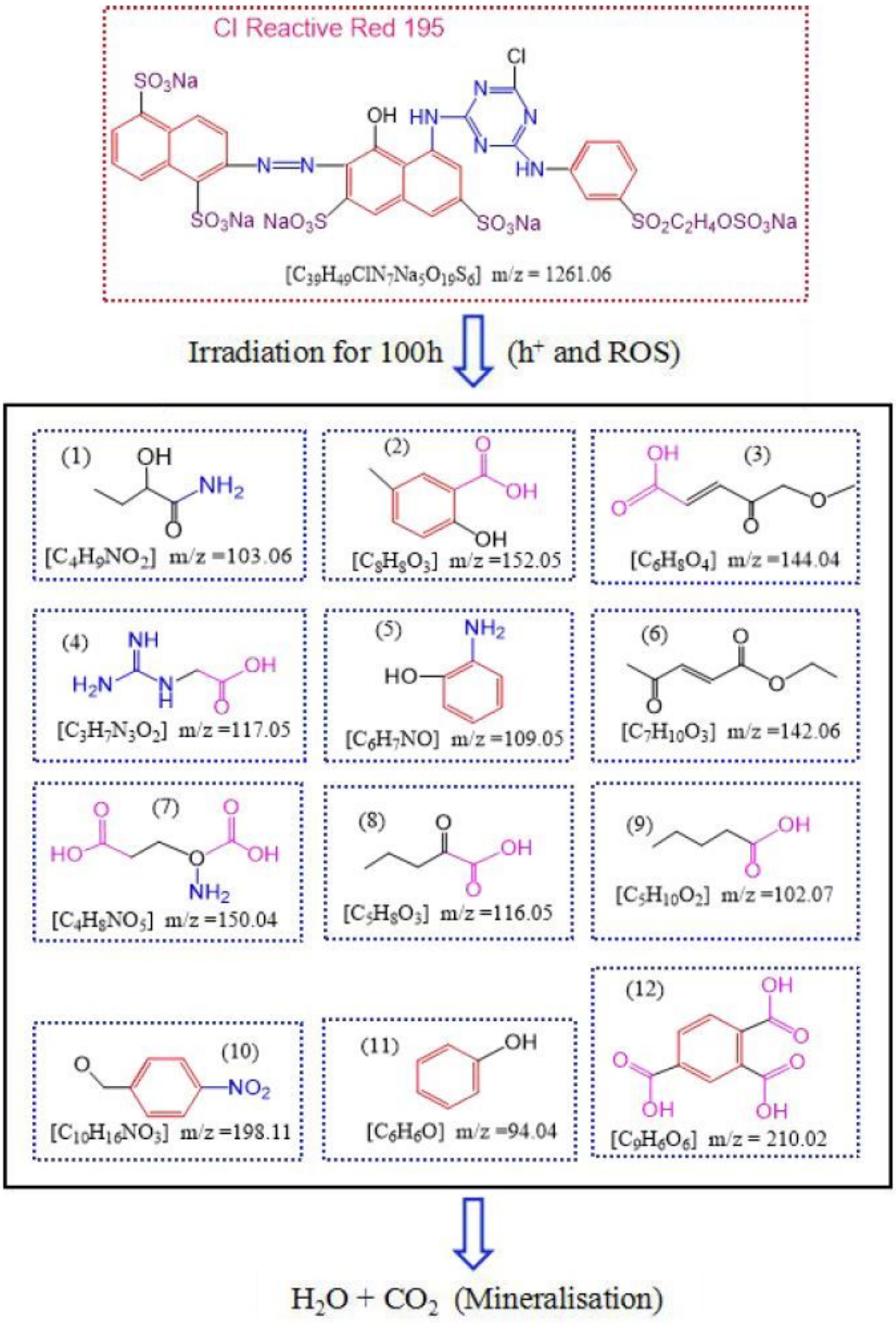

Figure 8

A proposed degradation route of RR 195 on Ag3PO4@CA-Cotton surface during the self-cleaning process

Supplementary Files

This is a list of supplementary files associated with this preprint. Click to download.

- scheme1.jpg
- scheme2.jpg
- scheme3.jpg